# A PHYSIOLOGICALLY ACCURATE MECHANICAL REPRESENTATION OF A RETROGRADE NAIL-BONE CONSTRUCT UNDER WALKING LOAD

by

Submitted to the Institute of Graduate Studies in
Science and Engineering in partial fulfillment of
the requirements for the degree of
Master of Science
in
Mechanical Engineering

Yeditepe University
2013

## A PHYSIOLOGICALLY ACCURATE MECHANICAL REPRESENTATION OF A RETROGRADE NAIL-BONE CONSTRUCT UNDER WALKING LOAD

APPROVED BY:

Assist. Prof. Dr. A.Fethi Okyar          .....................................
(Thesis Supervisor)

Assist. Prof. Dr. Koray K. Şafak         .....................................

Assoc. Prof. Dr. Can A. Yücesoy          .....................................

DATE OF APPROVAL: 21/01/2013

# ACKNOWLEDGEMENTS

# ABSTRACT

# A PHYSIOLOGICALLY ACCURATE MECHANICAL REPRESENTATION OF A RETROGRADE NAIL-BONE CONSTRUCT UNDER WALKING LOAD

Intramedullary (IM) nails have become a viable alternative in bone-distraction operations and treatments of long bone fractures. Upon stabilization of the fractured/dissected limb via the nail, the resulting construct accommodates the load bearing function of the otherwise healthy limb. In establishing design performance targets for these devices, *in vitro* test conditions are widely accepted leaving the *in vivo* conditions aside. However, *in vivo* device failures reported in both lengthening and fracture healing periods necessitate novel modeling considerations. In this thesis, it was aimed to identify mechanical conditions which IM nails are exposed to during distinct operational stages, and to predict the mechanical response of these devices more accurately in a finite element environment. In this regard, loads arising in limb distraction (SFM) was simulated in the first part of the study, as this brings the bone-implant construct to a totally different regime than the hip-joint contact force (PFM). The effect of loading type on load transmission paths through the locking pins was compared for two distinct loading modes, namely, SFM and PFM. In the second part of the thesis, the response of retrograde type intramedullary nail-implanted femur with a diaphyseal mid-fracture as well as the intact femur were investigated at the instance of maximum hip contact force of a gait cycle. The effect of different boundary and loading configurations on the mechanical behavior of the construct were identified.

# ÖZET

## RETROGRADE TİPİ ÇİVİ-KEMİK YAPISININ YÜRÜME YÜKÜ ALTINDA FİZYOLOJİK OLARAK DOĞRU MEKANİK TEMSİLİ

İntramedüler çiviler kemik uzatma operasyonlarında ve uzun kemiklerin kırık tedavilerinde geçerli bir alternatif olmuştur. Kırılmış/kesilmiş uzuvun çivi ile kararlı bir hale getirilmesiyle, oluşan yapı sağlıklı uzuvun yük taşıma fonksiyonunu üstlenir. Bu cihazların tasarım performansı kriterlerini oluştururken, vücut dışında gerçekleştirilen deney koşulları (vücut içindeki durumu bir kenara bırakarak) yaygın olarak kabul edilmektedir. Fakat, uzuv uzatma ve kırık iyileşme süresince rapor edilen vücut içindeki cihaz bozulmaları, yeni modelleme değerlendirmelerini gerekli kılmaktadır. Bu tez çalışmasında, intramedüler çivilerin çeşitli operasyon aşamalarında maruz kaldığı mekanik durumların teşhiş edilmesi ve sonlu elemanlar ortamında bu cihazların mekanik davranışlarının daha gerçekçi bir şekilde incelenmesi amaçlandı. Bu amaçla, tezin ilk kısmında, uzuv uzatma sonucu oluşan yükler (SFM)--bu yükler kemik-implant yapısını kalça eklemi temas kuvvetinden (PFM) tamamen farklı bir duruma soktuğu için--benzetildi. Yükleme tipinin sabitleyici vidalar vasıtasıyla yük aktarımı üzerine olan etkisi iki farklı yükleme modu için (SFM ve PFM) karşılaştırıldı. Tezin ikinci kısmında, diafizyel bölgede kırık içeren retrograde tipi çivi takılmış ve doğal uyluk kemiklerinin davranışları yürüyüş evresinin en yüksek kalça eklem temas kuvvetinin oluştuğu anda incelenmiştir. Farklı sınır koşulları ve yükleme konfigürasyonlarının yapının mekanik davranışı üzerine olan etkisi belirlenmiştir.

# TABLE OF CONTENTS

## LIST OF FIGURES

# LIST OF TABLES

# LIST OF SYMBOLS/ABBREVIATIONS

| | |
|---|---|
| A.S | Axial stiffness |
| B.C | Boundary condition |
| BIC | Bone-implant construct |
| B.S | Bending stiffness |
| C.S | Coordinate system |
| FEA | Finite element analysis |
| HCF | Hip contact force |
| HJF | Hip joint force |
| IM | Intramedullary nail |
| L.C | Loading condition |
| NPA | In vivo measurements in an average patient |
| PFM | Point force model |
| PCSA | Physiological cross sectional area of a muscle |
| SFM | Spring force model |

# 1. INTRODUCTION

## 1.1. INTRAMEDULLARY NAILING

Treatment of bone fractures and limb lengthening have been studied for years by scientists as there are thousands of patients suffering from these problems in the world. Orthopaedists and engineers are trying to find simple ways to overcome difficulties of lengthening human limbs and treatment of bone fractures. As a result of this pursuit, they developed some methods. One of these methods is most popular, widespread and widely used around the world, which is called as the intramedullary (IM) nailing technique. This technique have replaced traditional methods, (i.e. Ilizarov's frame and plate fixators), in the treatment of bone fractures and limb lengthening through the fast advancement in biomedical technology. The reasons of why this technique is more preferred than others, i.e. Ilizarov's frame and plate fixators can be summarized by several factors such as:

   i. It allows patients to carry on their modern-day living conditions in the post-operation and hospitalization periods [1],
   ii. it enables early fracture consolidation,
   iii. almost no pin site related infection problems arise,
   iv. intramedullary nails are true load sharing devices that bear the most of the loads in the bone during fracture healing and bone lengthening [2, 3].

Due to these advantages, intramedullary nailing technique is the perfect choice for leg lengthening operations and bone fracture treatments [1, 4]. Intramedullary (IM) nails are implants designed to fit into the medullary canal of a human femur (or tibia) to lengthen the limb or stabilize broken bone during fracture healing [5]. These devices are attached to the bone via locking screws/pins, passing through both bone and the nail. The screws provide stability to the system, and theirs effect on the mechanical behavior is critical [6]. The whole system consisting of bone, nail and the screws is called as bone-implant construct (BIC).

### 1.1.1. Types of Intramedullary Nails

Today, various designs of these devices are available in the market depending on the needs of patients. There are generally two types of intramedullary nails which are static and dynamic IM nail systems. Static nails are just stabilizers used for the treatments of diaphyseal and metaphyseal fractures of long bones. Examples of various static nails are shown in Figure 1.1. In the healing period, nail provides for alignment and orientation of the bone fragments, while allowing load transmission across the fracture site [3,6]. Different static nail models are used depending on the type of fracture, e.g. transverse, oblique, spiral, comminuted etc.



Figure 1.1. Various static interlocking nails. Adapted from [7]

Dynamic (distractor) nails are utilized not only as stabilizers, but also as limb lengtheners [8--11]. By virtue of telescopic motion between two mating parts, the device can extend axially inside a dissected bone, and elongate it to a desired length. Due to this telescopic motion, this device is also called as intramedullary telescopic nail. A schematic drawing of a dynamic nail is seen in Figure 1.2. Distraction in this dynamic nail is actuated by means of a miniature electrical drive system, which is energized and controlled from outside of the body without any direct physical connection or cabling [11].
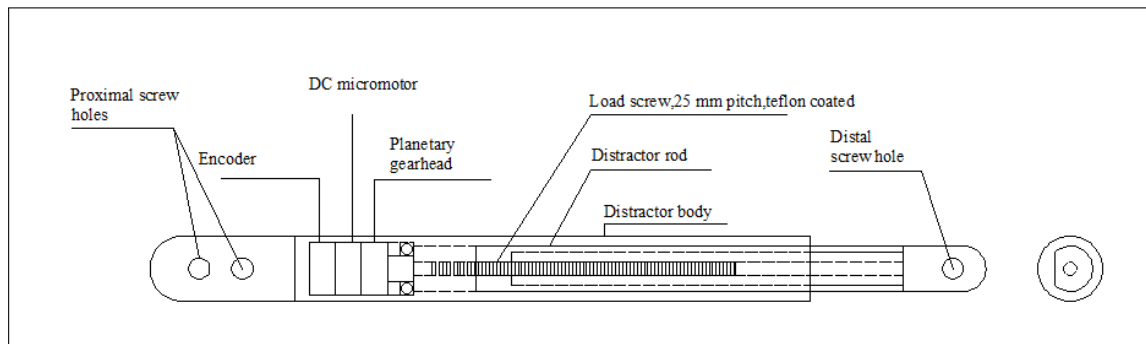
Figure 1.2. Schematic description of an intramedullary dynamic nail. Adapted from Okyar *et al*. [11]

Osteotomy operation (a surgical operation whereby a bone is cut to shorten, lengthen or change its alignment) is required in limb lengthening operations. This operation dissects the bone into two fragments. Certain factors are required for optimal bone regeneration and/or fracture healing [12--14]. Mechanical conditions at the osteotomy location/fracture site deeply affects the healing process. These conditions are a function of the stiffness of the construct used, the width of the fracture gap and, the nature and size of the external loads which the construct is exposed to. Insufficient stiffness of the construct can contribute to delayed fracture healing or sometimes non-union of the bone [14, 15]. Stiffness, in simple terms, can be described as the rigidity of a construct. It is found by the ratio of applied force in the construct to displacement produced by this force along the same degree of freedom. The performance of IM nails are evaluated based on the constructs' stiffnesses.

## 1.2. RATIONALE AND OBJECTIVE OF THE THESIS

Failure of IM nails were reported in several studies due to excessive bending on the locking pins and fatigue [16--18], bone re-fracture and nail failure [1, 15, 19, 20]. Design of these mechanical devices is critical to prevent such complications, and therefore should be based on *in vivo* conditions, i.e. physiological constraints and loading of the bone. This requires correct representation of *in vivo* loading conditions of these devices and anatomy, which in turn, lead to the production of safer implants. IM nails function under distinct operational phases from implantation to full recovery. This fact is usually overlooked during design cycle, leading to the misrepresentation in the mechanical behavior. These phases include lengthening, consolidation and fully healed state for a distractor nail; and consolidation and the fully healed state for a static nail. The mechanical circumstances significantly differ between each stage. However, in pre-clinical testing of these devices it is usually assumed that they operate in a fully healed state (device is tested under full weight bearing with an application of hip contact force alone). For instance, in the case of a distractor nail, internal forces arise due to the motions generated by the device during the lengthening [21]. Specifically, the increase of inter-fragment distance between osteotomized bones leads to generation of tensile forces in the callus and soft tissue and an equivalent amount of compressive force in the bone fragments [22,23]. This situation puts the construct in a totally different loading environment, which needs to be investigated specifically. As the distraction reaches about 10 % of the limb length, the reaction provided by the stretched muscles and ligaments become a primal load factor [24]. A maximum value of tensile force of nearly 1000 Newton (N) has been reported in patients with congenitally short limbs [25]. Although, it has also been reported that large amounts of force relaxation occurs after the peak value has been reached, the design may conservatively be based on the peak load. The way in which loads are transferred from bone to the IM nail is critical for the design of such devices, a better understanding of which may advance the production of safer implants.

The focus of this thesis is to identify the mechanical conditions which IM nails are exposed to and to predict the mechanical response of these devices more accurately in a finite element environment. In this regard, we first aimed to answer the arising question that: *In modeling a distraction process, how should the tissue load be correctly represented in order to obtain a better understanding of the mechanical response of IM nails during limb lengthening*? After answering the above question and digging more in the literature, we saw that there is

no standard of testing these devices. Some authors, (e.g. [26]) suggested applying walking loads in pre-clinical testing of femoral implants, as this loading configuration is one of the worst case scenarios for hip joint loading. This is supported by the work of Morlock et al. [27] which reported walking is the primary dynamic activity of a patient (10.2 %). Several boundary and loading conditions were employed in experimental tests [28--30] and numerical models [29, 31, 32] while investigating the mechanical behavior of the implanted and intact bone. Because there is no standard accepted procedure of applying boundary conditions (B.C) and loading conditions (L.C) in these tests, results show huge variations which makes it difficult to compare outputs of different studies. Therefore, it was aimed to shed light onto the following question in the second part that: *How should computational set-up be such that pre-clinical testing of these devices be performed to obtain a physiologically accurate mechanical response*?

## 2. LITERATURE REVIEW

### 2.1. ANATOMY OF HIP AND KNEE JOINTS

Femur is the longest and strongest bone in the body. Both ends of the femur (hip and knee) are joints meeting the parts in the skeleton which are pelvic bone in the proximal side and tibia in the distal side, respectively. The hip joint is like a ball and socket joint where the femur articulates with the pelvic bone and its primary function is to support the weight of the body in both static and dynamic postures. Femoral head is a round ball which fits inside the cavity of the pelvic bone called acetabulum (socket). A detailed picture of hip joint is seen in Figure 2.1.
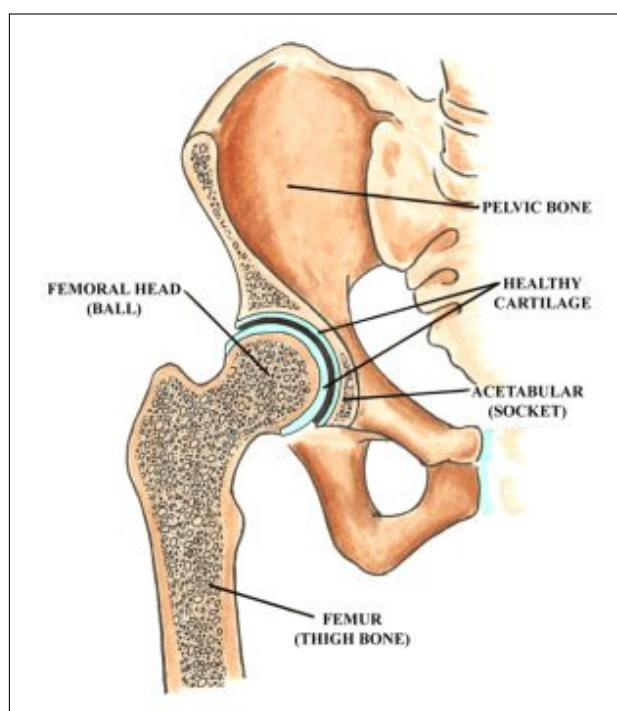


Figure 2.1. Anatomy of hip joint. Adapted from [33]

Femoral head and acetabulum are covered with articular cartilage which allows smooth and painless motion of the joint. Femoral head is connected to the socket by soft tissue and a ligament contained in the fossa of the acetabulum.

The knee joint is one of the largest joints in the body whose function is to provide mobility and

stability to the lower limbs. It is made up of three bones (femur, tibia and patella) and a variety of ligaments which connect bones to together. A complex structure of this joint is presented in Figure 2.2. The weight-bearing surfaces of the knee (distal end of the femur and proximal end of the tibia) are also covered with articular cartilage to provide a low friction surface for movement. Motion of the knee is controlled by several muscles and ligaments (collateral and cruciate ligaments). Collateral ligaments are located at two sides of the knee called medial and lateral collateral ligaments, and they stabilize the knee from side to side. Cruciate ligaments are found inside the knee joint making an $X$ with the anterior cruciate ligament (ACL) in front and posterior cruciate ligament (PCL) in the back. Cruciate ligaments control back and forth motion of the knee joint. In this joint, medial and lateral meniscus act to absorve shock at two sides of the joint between the cartilage surfaces of the femur and tibia.



Figure 2.2. Anatomy of knee joint. Adapted from [34]

## 2.2. MEASUREMENT OF FORCES IN THE FEMUR

The lower extremity provides locomotion and support to body via its musculo-skeletal system which includes bones, joints, tendons, muscles, ligaments and other structures. Muscular

Table 2.1. Muscles of the femur and their primary functions. Adapted from Britton [35]

| Muscle | Function |
|---|---|
| Sartorius | flexes, laterally rotates, and abducts the thigh at the knee |
| Rectus femoris | extends the leg at the knee joint |
| Vastus medialis | extends the leg at the knee joint |
| Vastus lateralis | extends the leg at the knee joint |
| Vastus intermedius | extends the leg at the knee joint |
| Iliacus | flexion and lateral rotation of the thigh |
| Psoas | flexion and lateral rotation of the thigh |
| Pectineus | adducts, rotates, and flexes the thigh at the hip joint |
| Adductor longus | adducts and flexes the thigh |
| Adductor brevis | adducts and flexes the thigh |
| Adductor magmus | powerful adduction of the thigh |
| Gracilis | adducts the thigh |
| Obturator externus | rotates the thigh laterally |
| Gluteus maximus | abducts, extends, and laterally rotates the thigh |
| Gluteus medius | abducts and medially rotates the thigh |
| Gluteus minimus | abducts and medially rotates the thigh |
| Tensor fascia lata | flexes and abducts the thigh |
| Piriformis | laterally rotates the extended thigh |
| Obturator internus | rotates extended the thigh laterally |
| Gemellus | rotates extended the thigh laterally |
| Quadratus femoris | rotates the thigh laterally |
| Biceps femoris | flexes the leg at the knee joint |
| Semitendinosus | flexes the leg at the knee joint |
| Semimembranosus | flexes the leg at the knee joint |

system consisting of all the muscles in body is one component of the musculo-skeletal system. Muscles keep bones in place and also play a vital role in movement of the bones whose motion is provided by the contraction of the muscles. Several muscles, functions of which are summarized in Figure 2.1, act on the femur [35].

It is obvious that muscles have some specialized functions, sometimes shared with other muscles, and are not necessarily active during every day activities [26,35]. ``The mechanical effects of a muscle are related in part to the size of the muscle and to its location relative to the joint it crosses'' [36]. Therefore, identification of muscle locations is important as well as the loads they apply to the skeleton. One can view the attachment regions of the femur muscles as shown in Figs. 2.3 and 2.4.
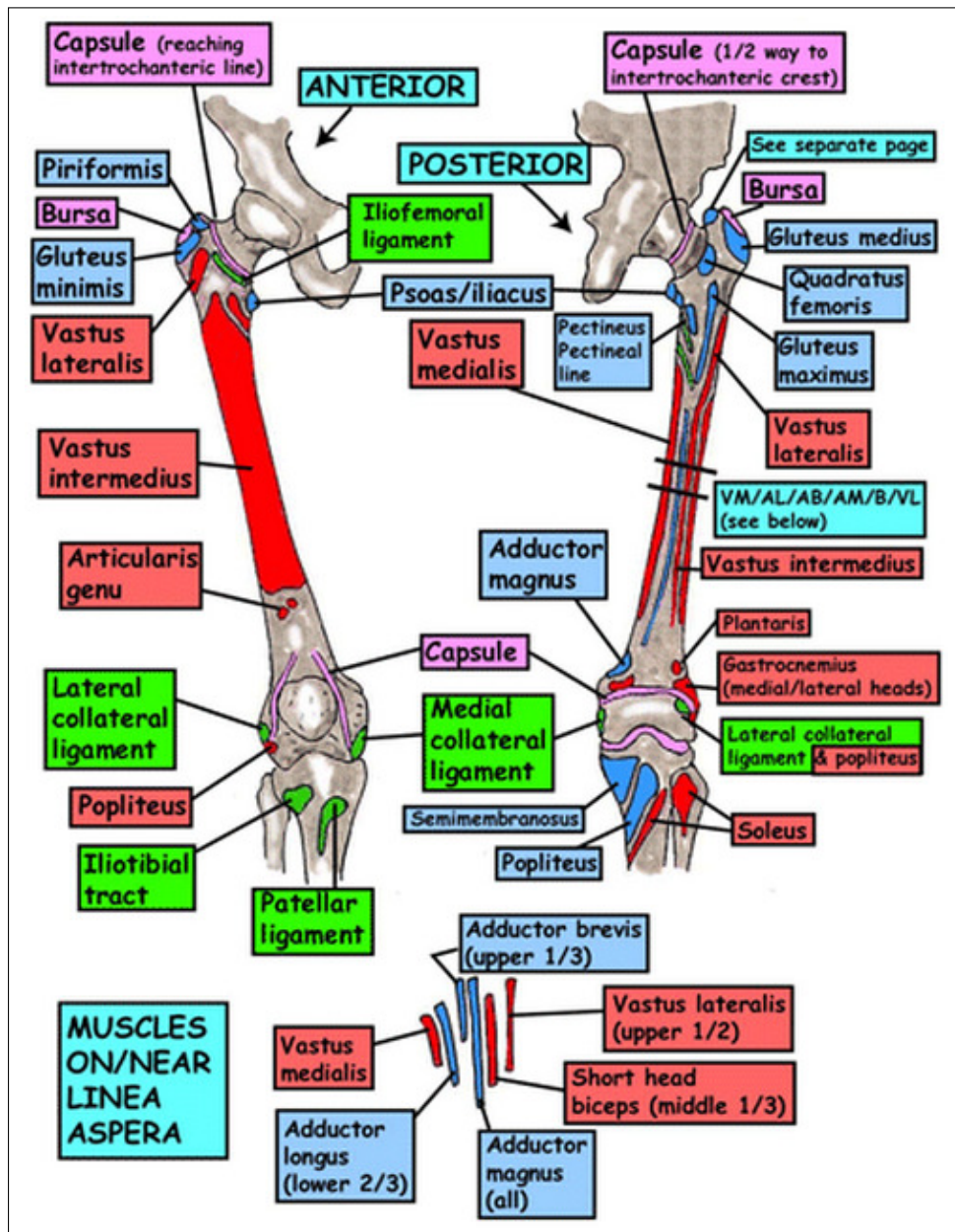
Figure 2.3. Muscle attachments of the right femur. Adapted from [37]
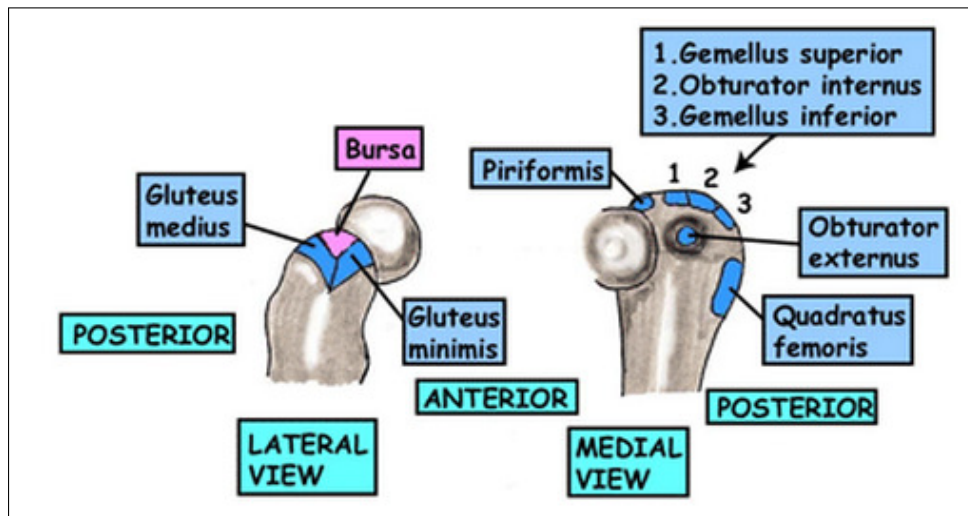
Figure 2.4. Muscle attachments of the right femur at the greater trochanteric region.
Adapted from [37]

``The forces that arise in the human skeleton are comprised of the body weight, ground reactions, inertial forces and internal forces'' [5].   ``Knowledge of the mechanical environment in the femur will provide a better understanding of the interaction between muscles and bones in general and supply basic information for more physiological boundary conditions in experimental and numerical investigations'' [38].  This knowledge is critical, and has been the subject of many researchers in the biomechanics community. Muscles exert considerable loads on the skeleton, effect of which can not be neglected, while performing their functions. However, non-invasive measurement of muscle forces is not possible due to ethical barriers. In the absence of appropriate force measuring devices, forces acting in the femur (muscle and joint forces) were estimated with some mathematical approaches [36,38]. Brand *et al*. [36] predicted muscle and hip contact forces in a living subject, via non-linear optimization techniques, during a gait cycle.  They included 47 lower limb muscles (using three data sets which were obtained from two cadaver specimens and a previous research) in their model.  It was argued in the study that muscle force predictions is sensitive to physiological cross sectional area of muscles, PCSA. Their calculations consisted of two parts.  In the first part, an inverse dynamic analysis was utilized to find intersegmental resultants, vector sums of the forces in all the structures (muscles, ligaments, joint surfaces) and the vector sums of the moments generated by these forces. The second part included the distribution of the intersegmental resultants to these structures.  After calculation of muscle forces by an optimization algorithm, joint contact forces were calculated by vectorially

subtracting the muscle forces from the intersegmental resultant hip forces. In another study [38], a three-dimensional model of the lower extremity was developed in an attempt to calculate internal forces in the femur during various stages of a gait cycle [38]. In that study, hip joint contact forces and moment distributions along the femur were calculated by performing static equilibrium equations in the lower extremity (taking into account all thigh muscles, body weight and contact forces at the hip, patello-femoral and knee joints). Results showed that ``muscles play a substantial role in balancing the loads within the femur'' (a load reduction in the femur up to 50 %) and bone is under axial loading rather than in bending.

The most reliable measurements of the *in vivo* hip contact forces with instrumented implants were performed by Bergmann *et al.* [26]. In that study, two types of instrumented hip implants with telemetric data transmission system, details of which can be found in [39,40], were used to measure hip contact forces. They reported hip contact forces (HCF) measured via their implant in four patients during the most frequent activities of daily living. These activities include walking (slow, normal and fast walking), going up and down the stairs, standing up, sitting down, standing on 2-1-2 legs and even knee bend. For each activity, measurements were reported as percentage of the body weight (BW) of each patient during the gait cycle. From the individual data sets, an average was calculated for each activity and these averages were used to define the measurements in an average patient (NPA). Because the data volume of measured contact forces and gait details was too large to include in that study, complete data as well as more details were contained in a compact disc ``HIP98'', which can be found in a website [41]. This group has also developed a software in which one can view the direction of the hip contact force relative to the femur as it is changing during the gait cycle, as well as the details about the patients, trials etc. A picture of this software is shown in Figure 2.5.

Hip contact force components for the average patient NPA during normal walking gait, reported in that study, is depicted in Figure 2.6. It is seen from the Figure 2.6 that femur is primarily under compression during the gait cycle (this inference is consistent with the previous results reported by Duda *et al.* [38]), and a peak value of HCP is read as 238 % BW when walking at a speed of 4 km/h.

This group has further developed a musculo-skeletal model of the lower extremity where they have calculated the hip joint force (HJF) and the muscle forces for walking and stair climbing [42]. In that study, muscle force distributions have been computed with a linear optimization
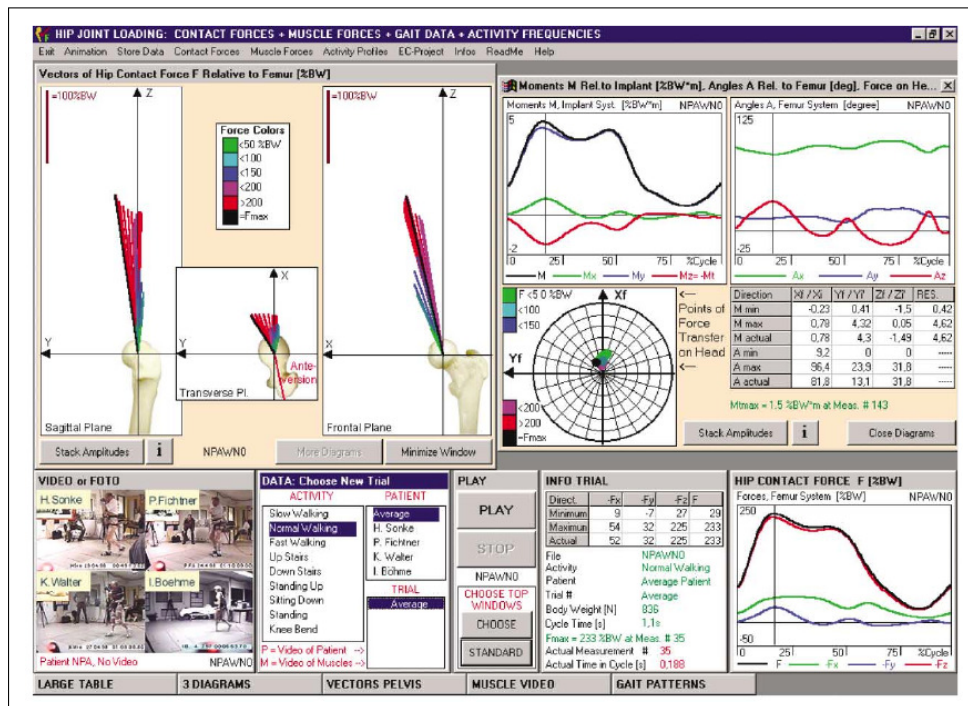
Figure 2.5. Screen shot of the `HIP98' software. Adapted from Bergmann *et al*. [26]
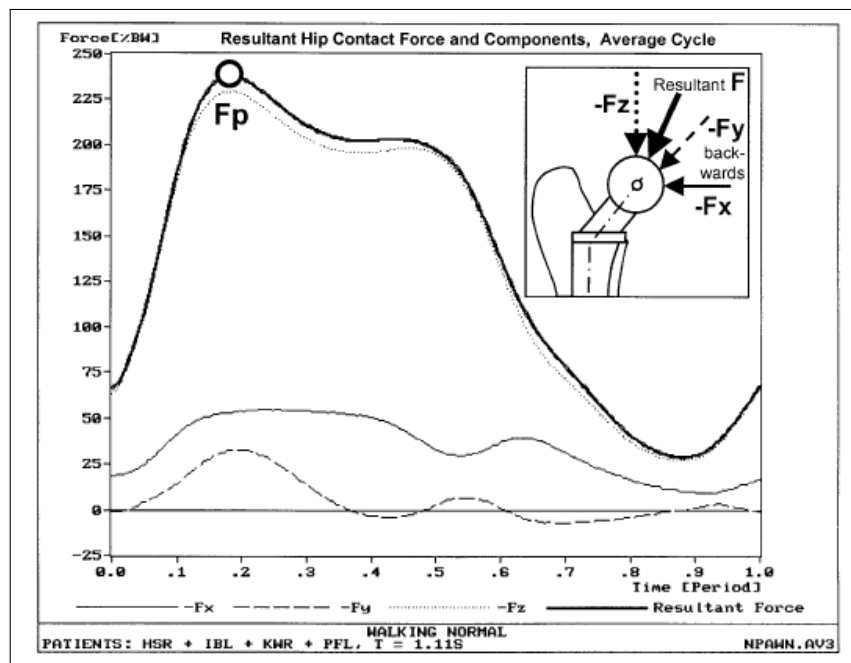


Figure 2.6. Typical average of the hip contact force and its components during normal walking (4 km/h). Adapted from Bergmann *et al*. [26]

algorithm, minimizing the sum of muscle forces (a common approach in literature to calculate muscle forces). They have later compared predicted hip joint force with measured *in vivo* hip contact force, and stated that their model can predict the *in vivo* HCP measurements of the experimental study [26] by a mean error of 12 % during walking and 14 % during stair climbing. With this model, for the first time, a cycle-to-cycle validation of predicted musculo-skeletal loading was realized.

In 2005, Heller *et al*. [43] suggested a load profile to be utilized in pre-clinical testing of femur implants. This load profile was the modification of their previous complex computer model of the lower extremity [42] which has been validated against *in vivo* data. Their old (complex) and new (simplified) models can be seen in Figure 2.7. In their simplified model (reduced-muscle loading), functionally similar hip muscles were grouped (gluteus maximus, gluteus medius, gluteus minimus as an abductor muscle with a single attachment site and adductus brevis, magnus, longus as adductor muscle), and then muscle and joint contact forces were computed through walking and stair climbing for an average of up to four patients. They reported that their simplified model can predict the peak *in vivo* hip contact force with an error of less than 10 % for a typical patient. It was discussed in that study that simplified load profile can be accurately used in pre- clinical testing and seems achievable in an *in vitro* test-set up.
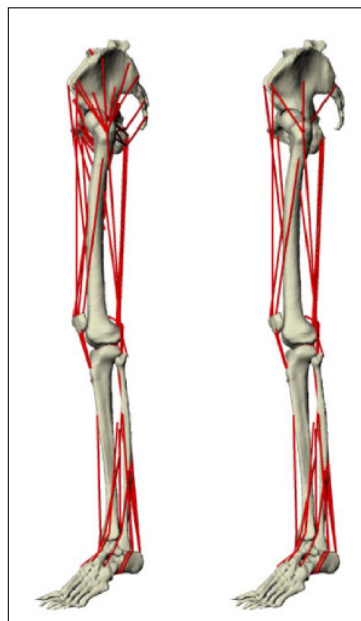


Figure 2.7. Comparison of the complex (left) and most simplified (right) models of the hip musculature. Adapted from Heller *et al*. [42]

## 2.3. LOADING OF THE PROXIMAL FEMUR IN NUMERICAL AND EXPERIMENTAL STUDIES

It has been a matter of debate in scientific community how to mimic physiological loading of the femur. Several research papers discussed whether the simulation of muscle loads is compulsory in pre-clinical testing of femur implants to obtain a physiologically accurate mechanical representation of the lower extremity [28, 31, 32, 38, 44--48]. Taylor *et al.* [44] tested the hypothesis that intact femur is loaded predominately in compression. Their study was composed of two parts: In the first part, they performed a finite element analysis (FEA) of the intact bone using physiological muscle (abductors, ilio-tibial tract and iliopsoas muscles) and joint contact forces (peak forces associated with the stance phase of gait were considered) to assess the mechanical environment in the diaphyseal region of the femur. In the second part, a radiological study was conducted to measure *in vivo* deflections of the femur during one-legged stance. The results showed that femur is loaded primarily in compression, and not bending (this is consistent with [38]) as previously thought. In addition, their FEA study revealed that a compressive stress distribution in the diaphyseal region can be achieved with physiological loading situation, but not with a simplified loading situation (joint reaction, abductors and ilio-tibial tract) which produced a bending stress distribution as reported in the literature. It was also reported in that study that the compressive load case led to negligible deflections of the femoral head.

Duda *et al.* [32] investigated the influence of muscle forces on femoral strain distribution at four phases (10, 30, 45 and 70 %) of a gait cycle using a finite element model of a human femur. They found that simplified load regimes (consisting of hip contact, abductor and ilio-tibial band forces) produced significant discrepancy in surface strains as high as 26 % in comparison to the load case including all thigh muscles. It was stated in the study that this difference is reduced to 5 % if the adductors are added to the simplified loading case.

An experimental study by Szivek *et al.* [48] examined the effect of lateral muscle loading on strains in the neck and diaphysis of the intact femur. Five hip loading configurations (see Figure 2.8), one with a HCP and abductor load only and four which incorporated lateral muscle loads as well, were compared in the study. It was reported in the study that the model consisting of HCP, vastus lateralis and ilio-tibial band loads in addition to the abductor load provided the simplest load configuration with a reasonable accuracy.
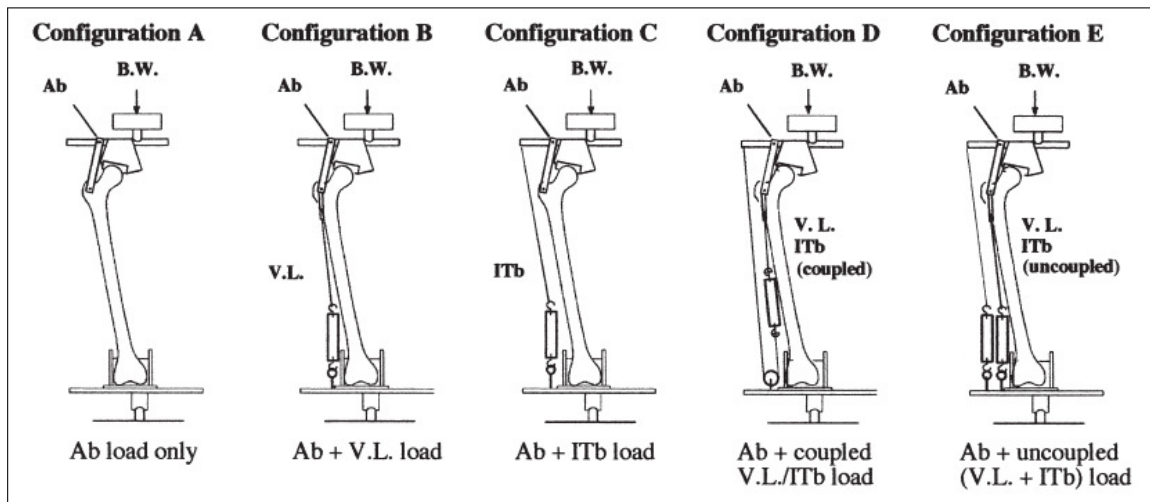
Figure 2.8. Femur loading configurations. Adapted from Szivek *et al*. [48]

Simoes *et al*. [28] examined the influence of muscle action and a horizontally constrained femoral head on the strain distribution within the intact bone (composite femur) in an experimental set-up. They tested three load configurations (joint reaction force only, joint reaction force plus abductors, and joint reaction force plus abductors, vastus lateralis and iliopsoas). In that study, strains were recorded for these three loading configurations via 20 uniaxial strain gauges placed on the proximal femur. Muscle force application locations and head constraining jig is shown in Figure 2.9. It has been stated in the study that application of muscle forces, i.e. abductor, vastus lateralis, iliopsoas reduced strain levels on all aspects of the femur. The study concluded that in the absence of detailed muscle force data, a constrained femoral head may represent a more physiological loading of the femur.

A finite element study by Polgar *et al*. [45] investigated the effect of simplified loading on strain distribution within the intact femur using the *Muscle Standardized Femur* model, and whether muscle forces could accurately be simulated by concentrated forces applied at the centroids of their attachment areas. In that study, nine load cases (at an instance of 10 percent of the gait cycle during level walking were considered. Results showed that simplified load cases generated non-physiological displacements and high strain magnitudes exceeding the physiological range of the bone. It was also stated that muscle forces could be accurately applied as concentrated loads if the results are discarded in the the vicinity of the load application locations. It was further stated in the study that precluding muscle forces or constraining the femur in mid-shaft leads to large non-physiological strain magnitudes.
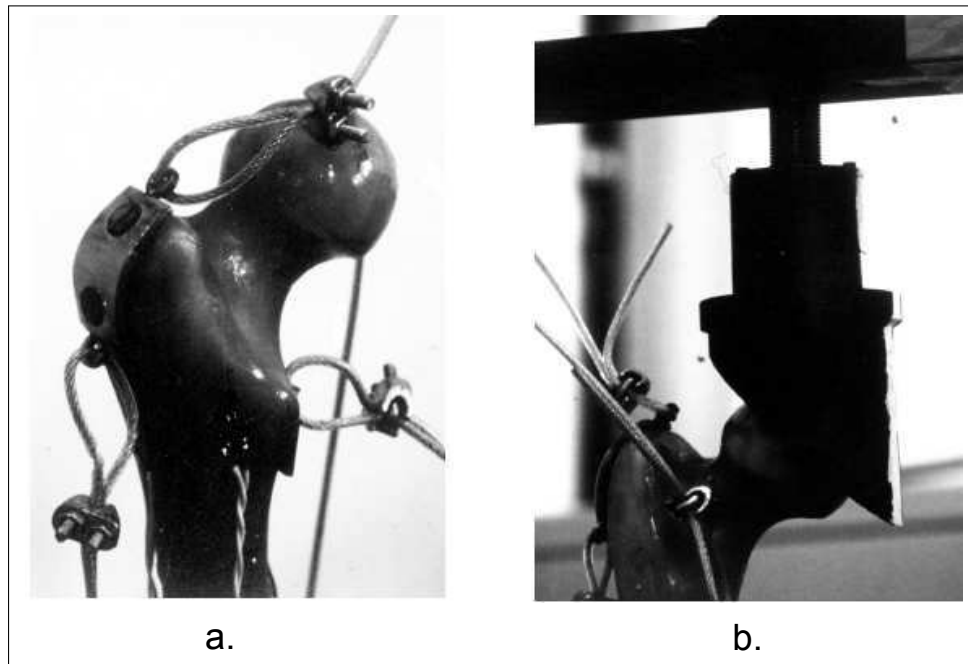
Figure 2.9. a. Plates and cables attached to the femur head for muscle force application and, b. device used to constrain the femur head horizontally. Adapted from Simoes *et al*. [28]

Speirs *et al*. [31] investigated the influence of different boundary and loading conditions on the principal strain distribution in intact femur. They argued that application of physiological boundary constraints can produce physiological deformation and straining of the femur, whereas non-physiological ones can not. Five boundary and loading cases were tested in a finite element model of *Standardized Femur*. Boundary and loading conditions applied in that study is seen in Figure 2.10. They used muscle and joint contact forces, which were estimated in [42] at the instance of maximum hip contact force occurrence, assuming a body weight of 860 N. It was shown in the study that only physiological boundary and loading conditions (case E in Figure 2.10 consisting of joint constraints at the hip and knee joints, and all muscles of the thigh) produced realistic deflections of the femoral head in both the coronal and sagittal planes. This observation was consistent with an *in vivo* study [44] which reported negligible displacement of the femoral head in one-legged stance position. Their study concluded that mode of loading substantially altered the strain distribution in the femur, which is significant for studies that examine fracture or bone remodeling simulations.

| Case | Loads | Constraints |
|------|-------|-------------|
| A | Simplified: HCF + gluteii | Diaphysis |
| B | Simplified: HCF + glutei + vasti | Diaphysis |
| C | Complex: JCFs + all muscles | Diaphysis |
| D | Complex: JCFs + all muscles | Condyles |
| E | Complex: JCFs + all muscles | Joint |
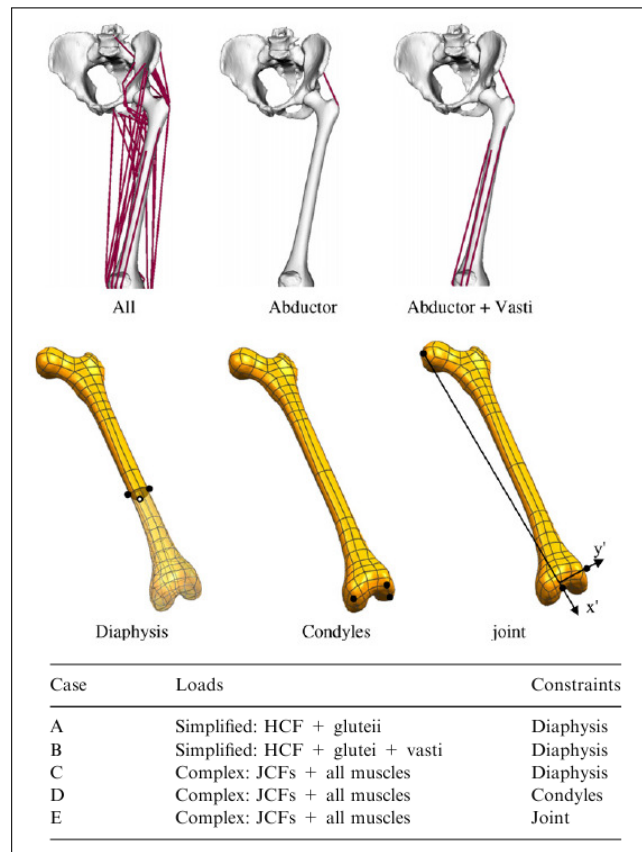
Figure 2.10. Schematic picture showing boundary and loading conditions applied in the finite element study. Adapted from Speirs *et al*. [31]

## 2.4. PRE-CLINICAL TESTING OF INTRAMEDULLARY NAILS

An enormous effort has been put in many biomechanical studies concentrating on comparing and characterizing various nails in the literature. A review paper by Eveleigh [49] highlights the conclusions of the most important of these studies. This review classified the mechanical properties of various nails in terms of bending, torsional and axial loading performance, and the configuration of locking screws in both stand alone and implanted (in cadaver and composite bones) configurations. Most of these studies, though useful for comparative purposes, focus on antegrade (i.e. inserted proximally to distally) nails, and consider only simplified loading (usually simulation of a hip contact force alone), in which details of stress in either bone or the nail is not included. The review concluded that further research was necessary about the load sharing characteristics in the bone-implant construct.

The mechanics and testing of intramedullary nails has been investigated in many experimental and finite element studies. While some of them [2, 6, 14, 30, 50] compare different nail designs (nail diameter, type, number and position of screws, type of fixation) by using axial, torsional and bending stiffnesses as performance criteria, a few focus on the load sharing characteristics of these devices [3, 29]. Moreover, some other studies examine the stress distribution in the nail and screws to understand the reason behind the failure of these devices [29, 51, 52]; and some proposed testing devices for biomechanical evaluation [53]. In these studies, usually, a fracture (generally a transverse fracture at the mid-diaphyseal region) is simulated in the femur prior to testing. The problems associated with these tests come out due to the oversimplified testing conditions, i.e. boundary constraints and loading. This situation creates a misrepresentation of the mechanical response predictions in these devices during design stage, which may lead to over or underestimate the design parameters.

A finite element study by Wang *et al*. [51] revealed the stress distribution in a Gamma nail and screws within a fractured femur under three loading conditions (L.C1: joint reaction force, abductors, ilio-tibial tract, iliopsoas; L.C2: joint reaction force plus abductors; L.C3: joint reaction plus abductors, but with different force magnitudes than L.C2). First two L.Cs represented the loading in a one-legged stance, while the third one did in stair climbing. They fully constrained the model at the distal end of the diaphysis. A picture of their model is depicted in Figure 2.11.

The effects of different fracture types (femoral neck and subtrochanteric fractures) on the stress distribution in the implant were investigated in that study. They assigned the elastic moduli for the cortical and cancellous bone as 17 GPa (outer surface through the shaft region), 1.3 GPa (ball of femoral head) and 0.32 GPa (region between ball of head and lesser trochanter), and for titanium as 114 GPa, respectively. A value of 0.3 was assigned to all the material Poisson's ratio. The results of their study showed that the presence of a subtrochanteric fracture caused more deformation than a neck fracture. In addition, it was seen that ilio-tibial tract and iliopsoas forces reduce the overall deformation in the construct. Moreover, insertion holes for the screws were reported to be the most critical areas of the construct based on the stress analysis. The study concluded supporting the advice by clinicians that it is satisfactory to omit one of the distal screws in simple fractures.
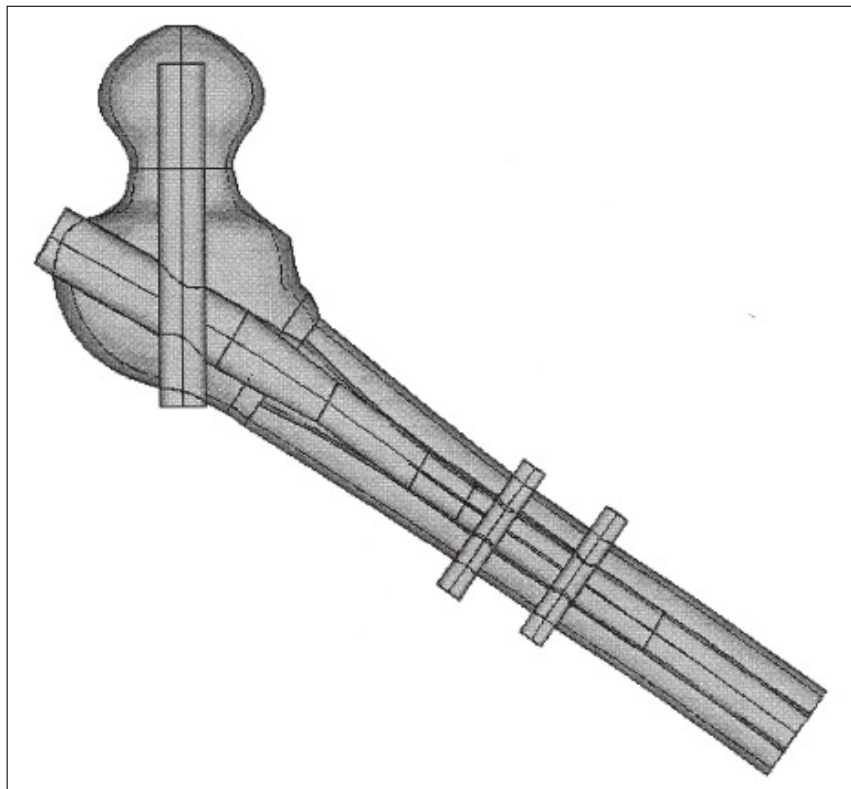


Figure 2.11. 3-D model of a Gamma nail within a fractured femur. Adapted from Wang *et al*. [51]

Schandelmaier *et al*. [30] compared several nail types of four unreamed solid nails and a slotted reamed nail in terms of axial, torsional and bending stiffnesses, mimicking comminuted mid-shaft fractures. A human cadaver femur was utilized in their experiments

with the simulation of 2 cm fracture gap. In axial and torque testing bone-implant construct was clamped in over the cast anchorage block as shown in Figure 2.12. For axial testing, a pre-load of 5 N and a maximum load of 1100 N was applied along femoral axis. Bending testing was carried out using a four-point bending test apparatus as presented in Figure 2.13. A bending load of up to 66 N-m was applied with a pre-moment of 0.05 N-m in their study. They calculated bending stiffness as the moment per degree of bending angle ($N - m/°$). Tested nail types are shown in Figure 2.14.
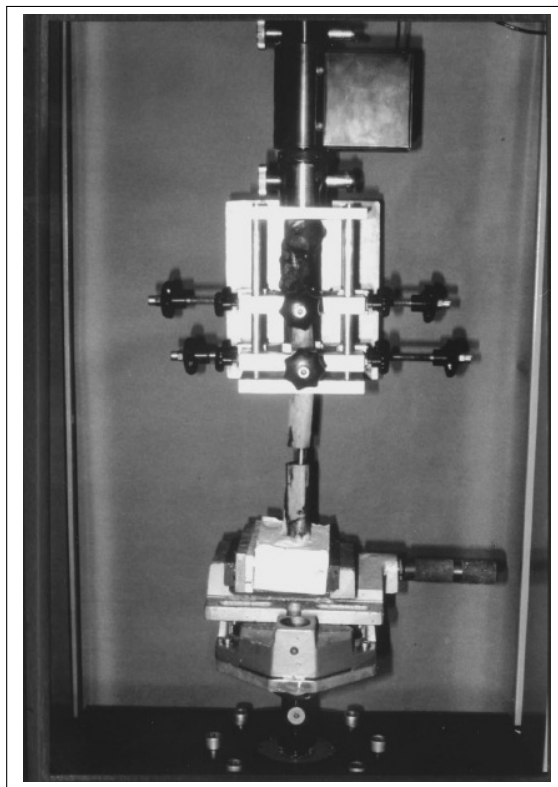


Figure 2.12. Axial and torque testing. Adapted from Schandelmaier *et al*. [30]
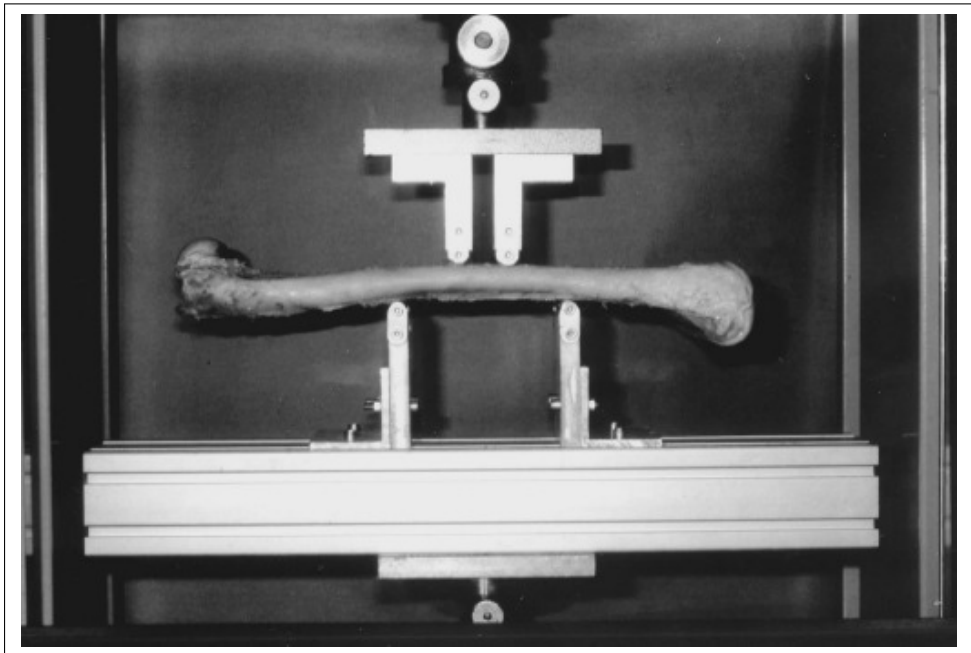
Figure 2.13. Four point bending. Adapted from Schandelmaier *et al.* [30]

Selection of different nail diameters and profile types allowed to decide the important factor for stiffness characteristics. It was stated in the study that the unslotted solid nail showed significantly more torsional stiffness compared to the slotted nail. It was also mentioned in the study that large diameter unreamed nail provided higher stiffness (32-68 %) in axial and bending testing. They completed the study by stating that stiffness of the BIC is more dependent on nail profile than on the press fit of nails in the medullary canal.

In 2000, Knothe *et al.* presented a new self-locking IM nail system [2]. The aim of their study was to test the handling and mechanical properties of two prototype nails in comparison to a conventional interlocking nail (see Figure 2.15). Two fracture models were generated as shown in Figure 2.16.a and Figure 2.16.b for distal and mid-diaphyseal fractures, respectively.

| Implant | Short form | Diameter (mm) | Profile thickness (mm) | Type of profile | Profile | Width of slot (mm) | Reamed up to (mm) | Distal locking | Material | Distributor |
|---|---|---|---|---|---|---|---|---|---|---|
| AO universal femoral nail | AOU | 11 | 1.2 | Tube slotted clover leaf | | 2.6 | 11.5 | 4.3/4.9mm | Stainless Steel | Synthes Mathys GmbH, D-44791 Bochum |
| AO Unreamed femoral nail 9 mm Steel | SUFN3.9 | 9 | – | Solid, round | | 0 | unreamed | 3.2/3.9mm | Stainless Steel | Synthes Mathys GmbH, D-44791 Bochum |
| AO Unreamed femoral nail 9 mm Steel | SUFN4.9 | 9 | – | Solid, round | | 0 | unreamed | 4.3/4.9mm | Stainless Steel | Synthes Mathys GmbH, D-44791 Bochum |
| AO Unreamed femoral nail 9 mm Titanium | 9TUFN | 9 | – | Solid, round | | 0 | unreamed | 4.3/4.9mm | Titanium Alloy (Ti-AL6-Nb7) | Synthes Mathys GmbH, D-44791 Bochum |
| AO Unreamed femoral nail 12 mm Titanium | 12TUFN | 12 | – | Solid, round, fluted | | 0 | unreamed | 4.3/4.9mm | Titanium Alloy (Ti-AL6-Nb7) | Synthes Mathys GmbH, D-44791 Bochum |

Figure 2.14. Tested intramedullary nails. Adapted from Schandelmaier *et al*. [30]
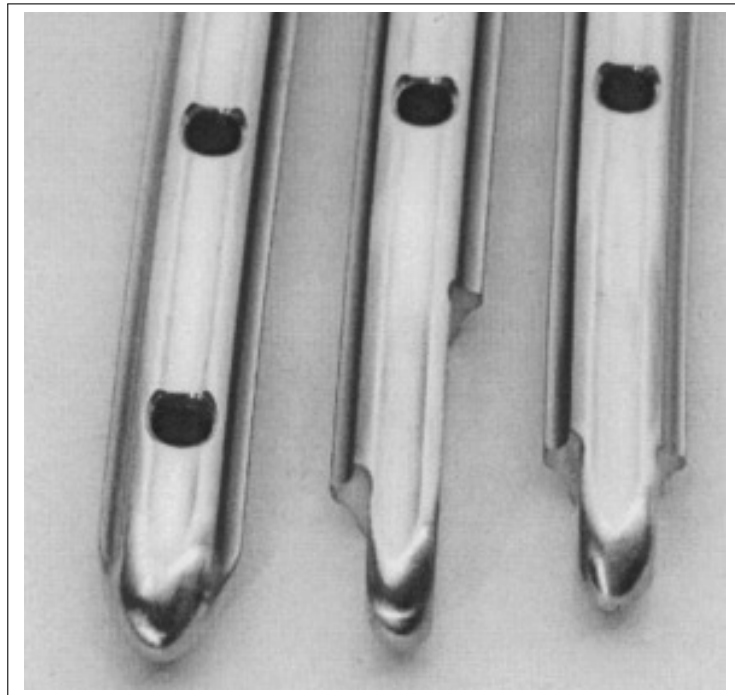
Figure 2.15. Left to right: Tips of the standard nail (Unreamed femoral nail (UFN) system of the AO group) and the two prototypes, respectively. Adapted from Knothe *et al*. [2]

These three nails were tested under axial compression and bending loads. In axial loading, bone-nail construct was placed as shown in (b) of Figure 2.17 such that loading was free of bending effects. Loading was carried on until either the osteotomy gap was closed or the system failed. They reported axial load-deformation curves for each bone-nail construct. In four bending test, BIC was positioned into the test fixture as depicted in (a) of Figure 2.17. The cross head was adjusted to produce a mid-shaft displacement of 0.2 cm at a rate of 2 mm/min, and they recorded moment versus mid shaft displacement during testing. In that study, bending stiffness was defined as bending moment per linear displacement of the loading point (Nm/mm), contrary to the definition of Schandelmaier *et al*. [30]. They showed that prototype 1 demonstrated a slightly higher bending stiffness than prototype 2 (right one in Figure 2.15), with symmetrically offset locking bolts. Results indicated that the mean axial failure load was 3360 N and 3180 N, for prototypes 1 and 2, respectively. It was discussed in the study that assuming an average body weight (717 N), all bone-nail constructs could withstood more than three times body weight under the axial loading until failure.

Gaebler *et al*. [53] proposed a new modular testing system for biomechanical evaluation of tibial intramedullary fixation devices as shown in Figure 2.18. This testing system
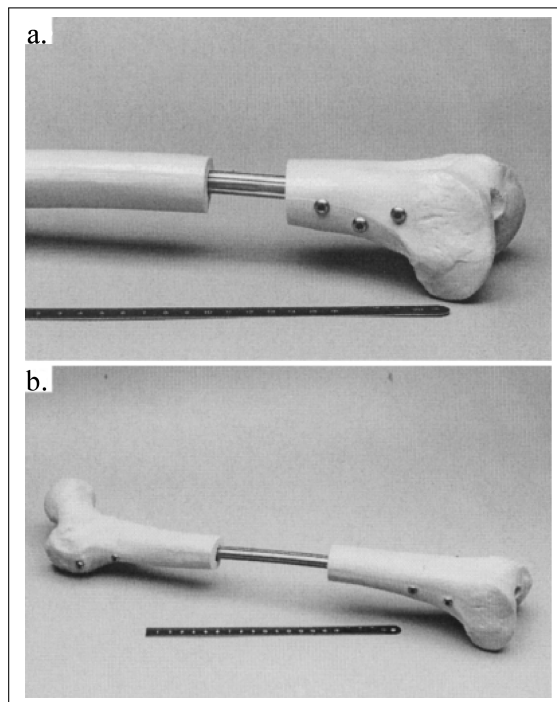
Figure 2.16. Fracture models, a. distal fracture 2 cm, b. mid-diaphyseal fracture 10 mm.
Adapted from Knothe *et al*. [2]
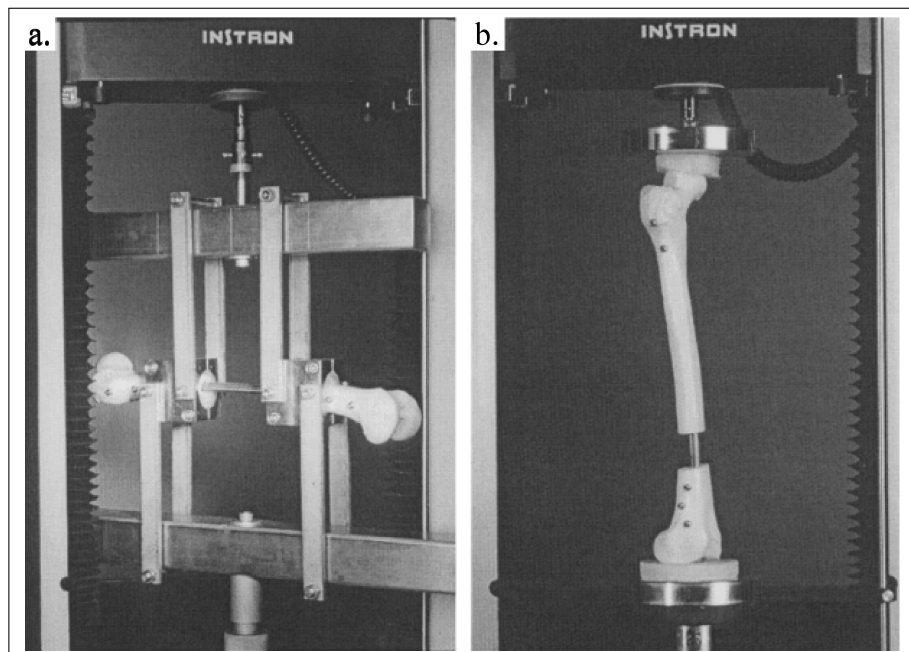


Figure 2.17. Mechanical testing set-ups, a. four-point bending, b. axial compression.
Adapted from Knothe *et al*. [2]

was designed to simulate a tibia and removal of the some modules mimics defect zones of the bone. It was claimed by the authors that ``their biomechanical study established a standard technique for the biomechanical testing of tibial nails, in a clinically relevant manner, avoiding the inconsistency of cadaver bone tests".

A finite element analysis of a femoral retrograde-intramedullary nail was done by Cheung *et al.* [3] at four stages of gait cycle. FEA results were verified with an experiment--performed by the same authors--in which BIC went under an axial compression load as shown in Figure 2.19. With respect to the loading, the study included 33 separate muscle and joint contact forces in FEA, but only a hip contact force in $11°$ adduction position (axial compression load) was applied in the experimental part. In both FEA and experimental part, femur was fixed distally in their study. Forces and moments carried by the bone and the nail were presented during four stages of the gait in that study. Load sharing between bone and the nail was discussed based on the force and moment measurements. Screw and screw holes both in the bone and the nail were identified as the most critical regions according to Von Mises stress distributions. However, it is important to emphasize that their results are only valid after a complete bone union as the study did not simulate any fracture.

A study by Chen *et al.* [6] employed both mechanical testing and FEA to examine the stiffness behaviors of different retrograde-nail bone constructs which are used in the treatment of distal femur fractures. Finite element models were utilized to estimate stress distribution around the screw holes. Two distal fracture models were simulated in the study as shown in Figure 2.20. The effect of screw number and position was investigated using axial and torsional stiffnesses as performance indicators. Compression and torsional experiments were conducted in the study, see Figure 2.21.

In both mechanical testing and FEA, femur was fully constrained at its distal end, and only a compression load (making a $7°$ with the femoral shaft and nail axes) was applied at the femoral head. The maximum load for compression was 1000 N with a constant displacement rate of $0.05$ $mm/s$ in their study. The results of that study indicated that an additional perifracture screw had the ability to increase stiffness by $40$ % for obliquely fractured bone (in compression and torsional loads), but it did not change stiffness in transverse fractures. In addition, it was said by the authors that screw position was more important than screw number. Moreover, it was discussed in the study that distal screw performed a more critical
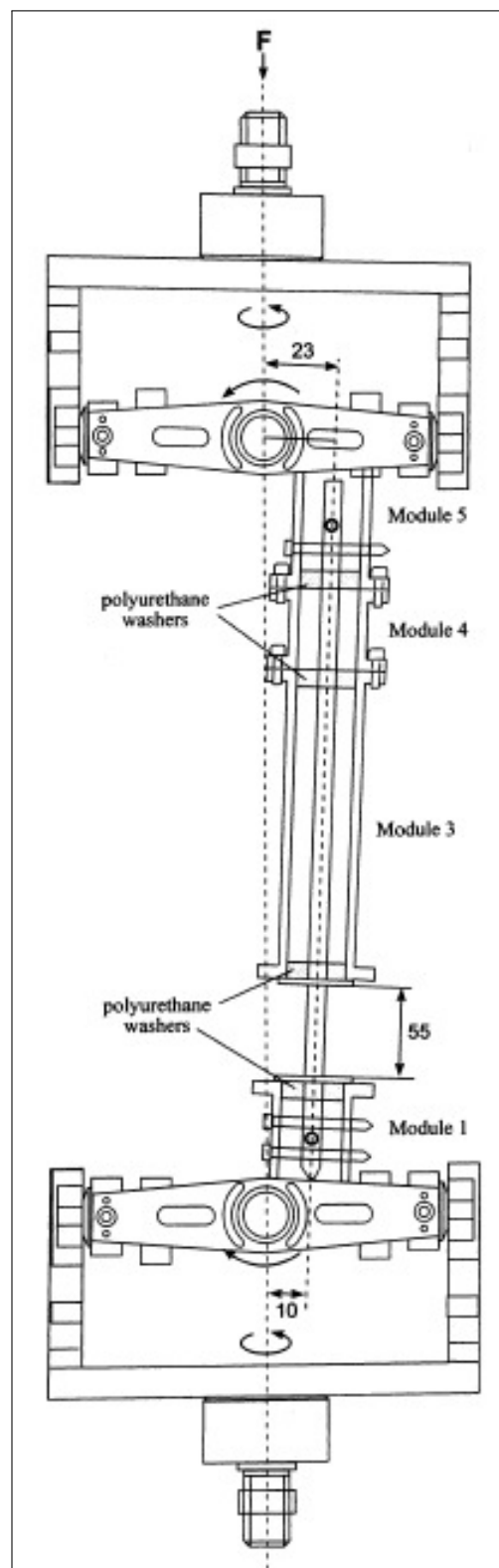
Figure 2.18. Testing device consists of five modules. Adapted from Gaebler *et al*. [53]
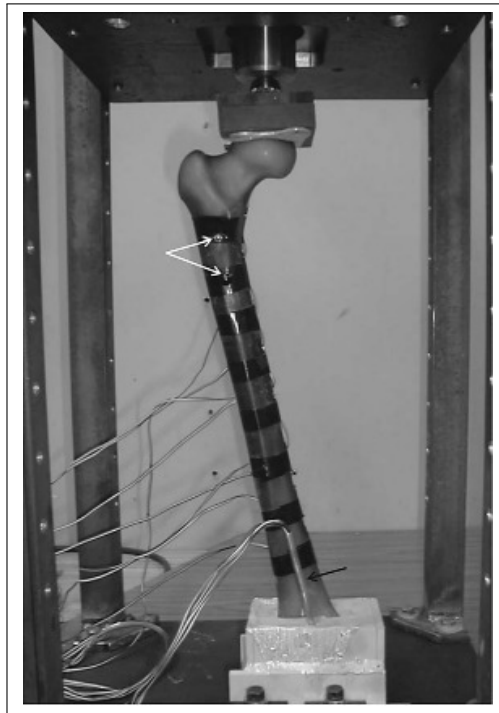
Figure 2.19. BIC axial compression testing where 8 strain gauges were attached to the bone with black tapes. Similarly, six strain gauges were located in the nail. Adapted from Cheung *et al*. [3]
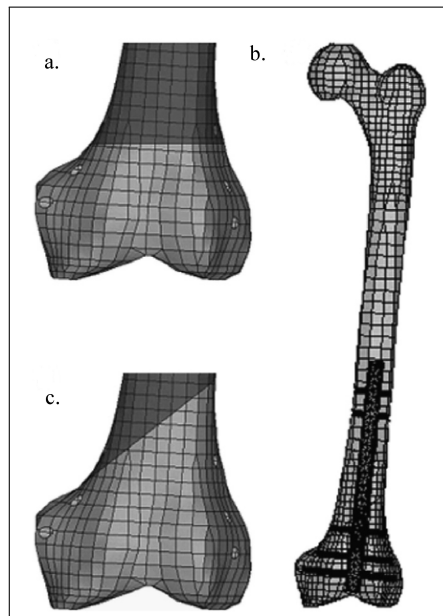


Figure 2.20. a. simulated distal transverse and b. oblique fractures. The circle holes represent screw positions. c. Meshed view of the bone-implant construct. Adapted from Chen *et al*. [6]

function in the construct than did the proximal screw.

Penzkofer *et al*. [14] tested the hypothesis that the use of a larger diameter IM nail together with compressed interlocking would enhance primary stiffness and reduce fracture site movements. Six pairs of human cadaver tibiae were used in the experiments and two nails (9 and 11 mm in diameters) were tested under axial tension/compression, torsion, four-point bending and shear loads. The nails were used in two interlocking modes, i.e. static interlocking and dynamic compression. One can view the tests performed in that study and the construct in Figure 2.22.
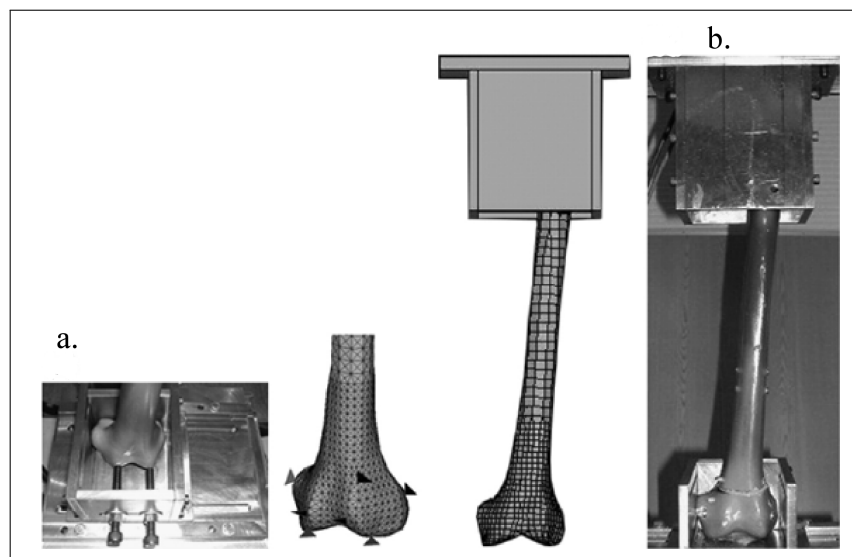


Figure 2.21. a. Distal portion of femur was constrained by screws at the anterior and posterior aspects in both mechanical testing and FEA, b. BIC with a transverse fracture in a testing machine. Adapted from Chen *et al*. [6]

A 8 mm wide fracture gap was created by the osteotomy operation in the mid-diaphysis of the tibiae bone. Results revealed that with static interlocking, the 11 mm diameter nail provided notably greater reduction of fracture site movement, compared to 9 mm diameter nail. In addition, stiffness of the construct was increased between 20 % and 50 % using 11 mm diameter nail. Lastly, it was seen in the study that dynamic compression feature of the nail decreased the inter fragmentary movements at the fracture site by 79 %. The study concluded suggesting the use of largest possible nail diameter with minimal reaming to minimize fracture site movement.
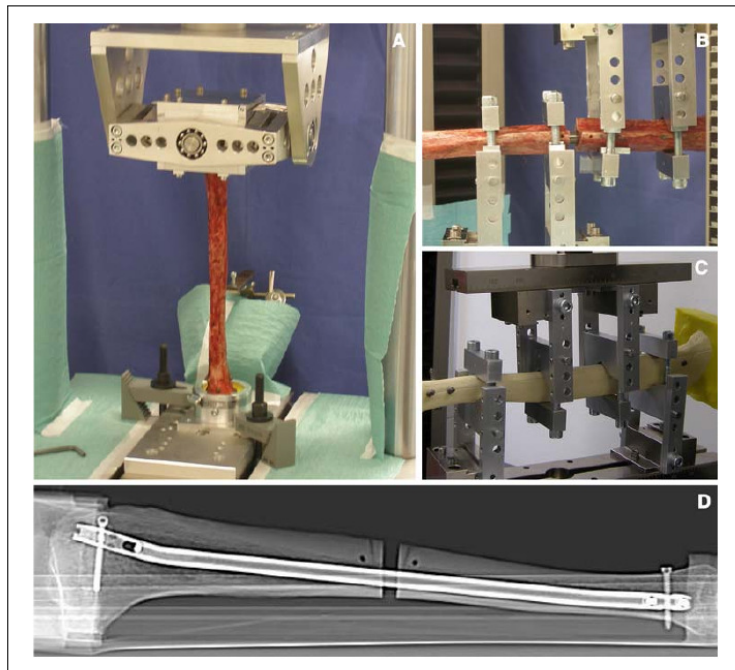
Figure 2.22. a. Tension/compression and torsion test, b. shearing test, c. bending test, d. tibia-IM nail bone construct with 8 mm mid-diaphyseal fracture. Adapted from Penzkofer *et al*. [14]

# 3. METHODS

This chapter of the thesis consists of two parts to answer the imposed questions discussed in section 1.2. Each part includes associated finite element models, loading configurations and explanations, respectively.

## 3.1. STUDY 1: IN MODELING A DISTRACTION PROCESS, HOW SHOULD THE TISSUE LOAD BE CORRECTLY REPRESENTED IN ORDER TO OBTAIN A BETTER UNDERSTANDING OF THE MECHANICAL RESPONSE OF IM NAILS DURING LIMB LENGTHENING?

### 3.1.1. Finite Element Model Considerations

A simplified model of the IM nail prototype, developed at the biomechanics laboratories of the Yeditepe University is presented in Figure 3.1. The nail consists of two parts, one stationary containment for the encoder-motor-gear assembly on the left, and a telescopic rod which provides distraction on the right [5]. The containment has a tubular shape of 12 mm outer diameter and 9 mm inner diameter, and it is 170 mm in length. The telescopic rod is 130 mm in length and 9 mm in diameter. Three interlocking pins, provide for the fastening of the IM nail with the bone segments; two of which were located on the stationary side, while only one pin was provisioned for the telescopic part. All pins are 6 mm in diameter.
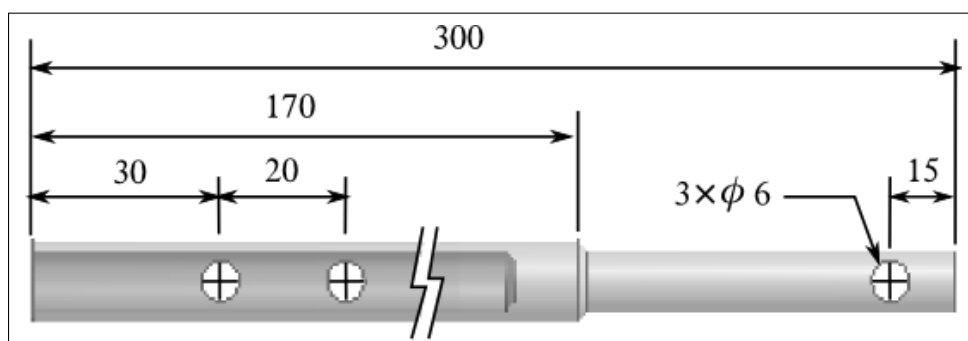


Figure 3.1. Simplified model of the IM nail

The model of bone-implant construct is shown in Figure 3.2. In this figure, the deformed state of the construct is seen as well as the undeformed one. An osteotomy gap of 2 mm

was inserted in the diaphyseal region of the femur, simulating a transverse osteotomy condition. The interlocking pins that provide for the mechanical fastening between the bone and the implant were located in the medio-lateral direction. The implant was concentrically positioned in the intramedullary canal, such that a gap of 3 mm occurs at the narrowest range before the load is applied, and the gap closure is automatically accounted for by the software upon loading. The longitudinal axis ($z$) of the model coincides with the anatomical axis of the femur in its undeformed state. The location of osteotomy, $D$, separates the femur into two segments--distal and proximal--corresponding to the left and right pieces, respectively. The amount of bending--denoted by $\theta$--is the change in rotation of the anatomical axis measured at $G$ about the $y$-axis.
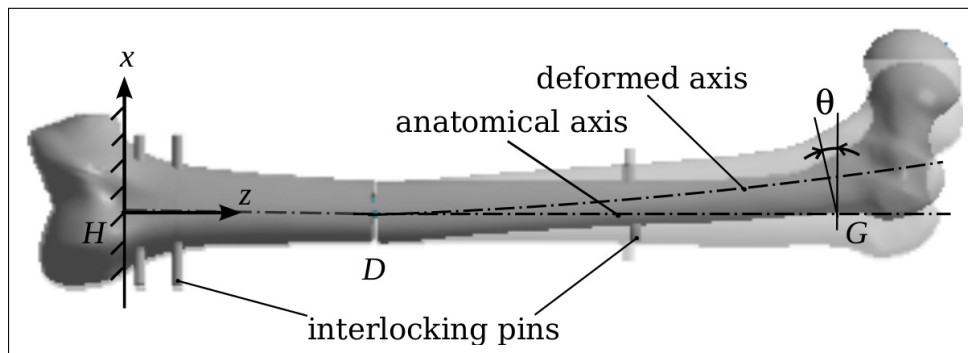


Figure 3.2. The bone-implant construct

### 3.1.2. Loading, Boundary Conditions and Construct Configuration

In this part of the thesis, we aim to provide a better model for the loads associated with tissue distraction. Previous models (testing performance of intramedullary implants) have largely relied on applying the loads--no matter what their sources may be--at the hip joint. (The loading direction in these tests, e.g. [6] were usually taken to have 7° with the femoral axis which corresponds to standing on one leg according to [26], but with a lower magnitude of hip contact force). However, correct representation of loading conditions corresponding to various stages in the life cycle of an implant (operation, lengthening, consolidation, dynamization, etc.) is thought to be an important factor in the accuracy of the constructs' mechanical behavior. For example, the peak distraction force attained at the end of lengthening defines a critical stage in the life cycle. Here, we propose to model the tissue load by three self-equilibrating springs equally spaced around the circumference,

almost parallel to the anatomical axis and equally sharing a total load of 1000 N (model labeled (a) in Figure 3.3), called the *spring-force model* (SFM). The second loading mode is called the *point-force model* (PFM, (b) in the same figure), which used the hip-joint force as its basis. Its magnitude is $1000 \ N$, similar to SFM case. Direction of the hip-joint force was taken as $\alpha=7°$ with the femoral axis--as is customary in *in vitro* test setups--constrained within the mediolateral plane. The antero-posterior component of the load was neglected in this study for the sake of brevity. The force magnitude of $1000 \ N$ was chosen based on the study of Simpson *et al*. [25], and also due to the application of similar force magnitudes applied in axial-compression testing of IM nails. This allowed us to compare our results with other studies in the literature.

In addition to these two loading modes, a pure bending moment of 55 N-m (on the mediolateral plane) was applied at the femoral head to obtain the constructs' bending stiffness. In all loading configurations, the construct was rigidly fixed at the distal end of the femoral diaphysis ($H$), representing *in vitro* conditions encountered during compression tests [6, 14, 30, 50, 54].

Distraction over the IM nails is realized via either an antegrade or a retrograde-type fit, in which the distractible nail is inserted through the hip or the knee, respectively. Related to both types of nailing, several advantages and disadvantages were reported in [55, 56], which necessitates analyzing both cases separately. As shown in *(c)* of Figure 3.3, the fixation between the nail and the bone was achieved by means of locking pins located at points $A$, $B$, $C$ for the antegrade configuration, and $D$, $E$, $F$ for the retrograde *(a)* and *(b)* in the same figure. All pins were rigidly fixed to the bone, while allowing relative rotation with respect to the nail. In the antegrade-type fit, the pins at $A$ and $B$ remained in the proximal side of the bone while the one at $C$ remained in the distal side. Thus, the load transfer between the bone and the nail occurred between points $A$ and $B$ in the proximal segment, and around point $C$ in the distal segment. Similarly, in the retrograde-type fit, points $D$, $E$, and $F$ were regions around which loads were transferred.
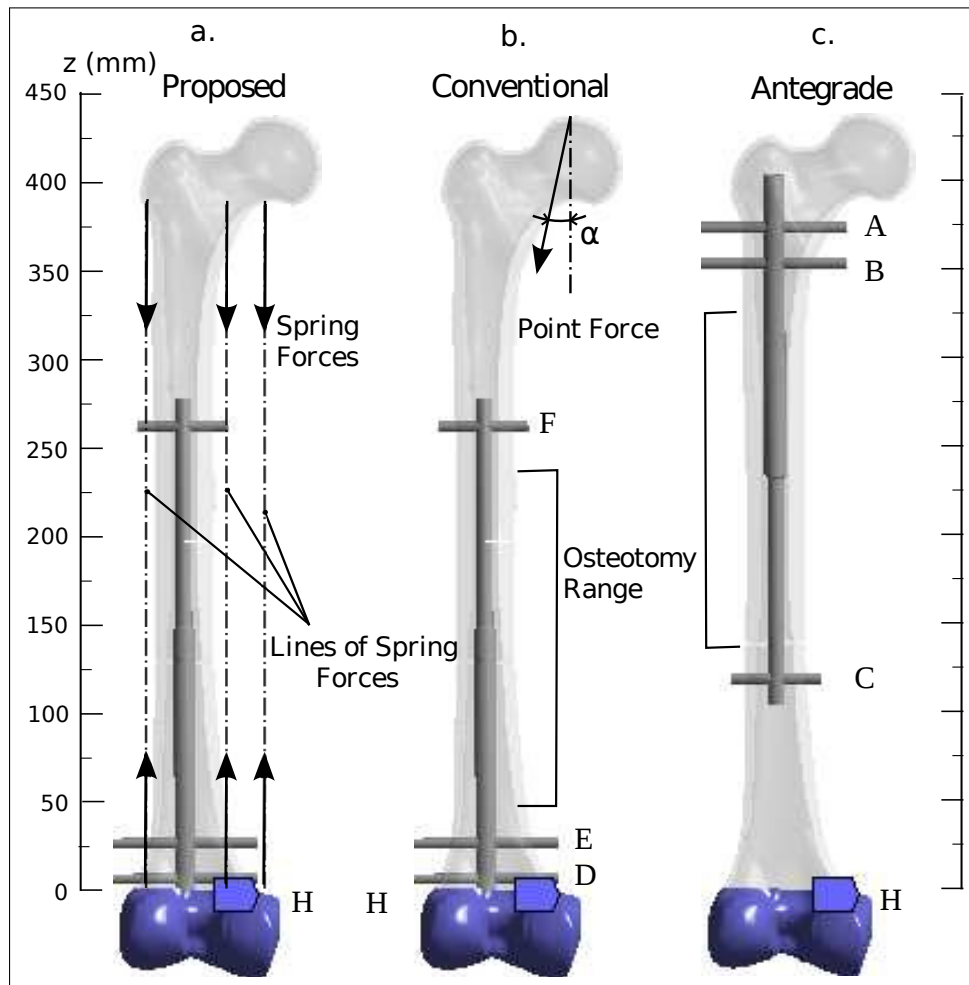
Figure 3.3. Loading and fitting configurations used in the finite elements analysis, a. the spring-force model, b. the point force model, and c. antegrade-type model, respectively. (Note that a. and b. are of retrograde-type fits)

### 3.1.3.  Finite Element Analysis

Finite element analysis is a widely accepted method for studying the mechanical performance of biomedical structures [3,51,57]. The modeling of the bone-nail construct was implemented in ANSYS 12.1 [58]. The third generation 3-D solid model of the femur obtained from [59] was used. In order to reduce computational effort, the cancellous portion --whose elastic modulus was only a small fraction of that of the cortical bone-- was removed from the model. The nail and pins were made of 316L grade steel. All the constituents were assumed to behave in a linearly isotropic fashion. Material properties are provided in Table 3.1.

Table 3.1. Mechanical properties of all the constituents of the bone-implant construct model

| Region | Elastic Modulus, $E$ (GPa) | Poisson's Ratio, $\nu$ |
|---|---|---|
| Nail (316L steel) | 200 | 0.33 |
| Bone (cortical) | 17.4 | 0.25 |

All the solid bodies were meshed with 20-node hexahedral (SOLID186) and 10-node tetrahedral (SOLID187) elements. Mesh refinements were applied at load transfer paths, contact and stress concentration regions. On average, the two femoral segments were discretized by a total of about 58,000 elements, the nail by about 69,000 elements, and the pins by about 3,600 elements. The meshed view of the bone-implant construct is shown in Figure 3.4. A total of roughly 162,000 finite elements and 320,000 nodes were used in the entire model.
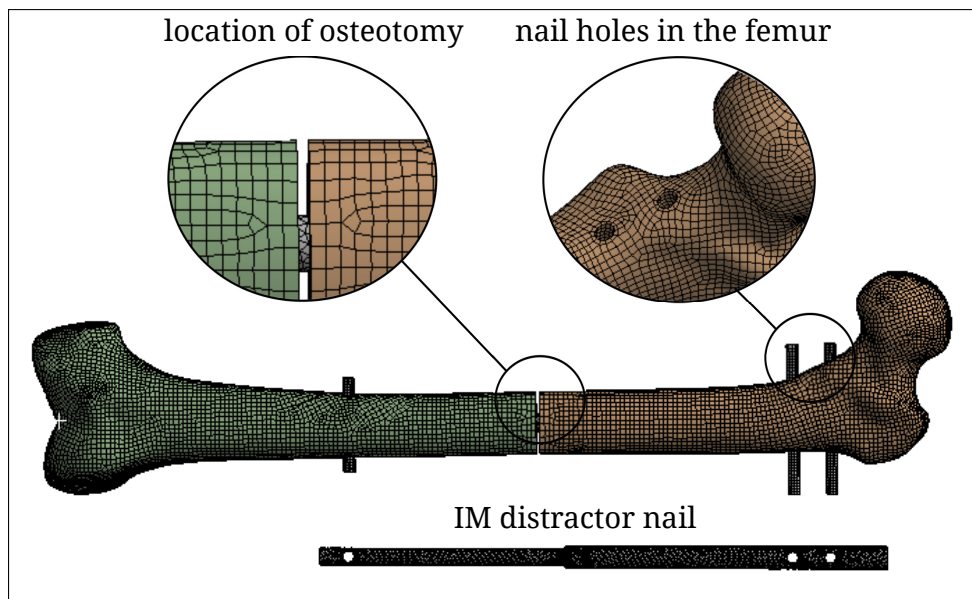


Figure 3.4. Meshed view of the bone-implant construct

Relative rotation between the nail and the pins was achieved through the use of revolute joint elements that are available in ANSYS. Three revolute joints were used in each model, corresponding to the three pin locations. The three springs used in the SFM models were preloaded by (333.3) N each. The spring stiffnesses were given as $(10^{-3})$ N/mm so as not to change the overall stiffness of the bone/implant construct.

In order to predict contact between the interior surface of the intramedullary canal and the outer surface of the nail, frictionless 8-node surface-to-surface contact elements (about 16,000 CONTA174/TARGE170 pairs) were used. The frictional forces between the nail and the IM canal have been neglected, however, normal contact forces restrict penetration at the nail/bone interface. The contact element pairs were adjusted to initially touch each other. The locking pins were embedded in the femoral cortex by bonded contact condition.

Upon running a series of finite element analyses, the bending moments transmitted via the locking pins were read from joint probes available in ANSYS. The required stiffness values had to be extracted from the output. The bending stiffness (B.S) was evaluated as the ratio of the (pure) mediolateral bending moment $M_y$, to the relative angle of rotation in the diaphyseal region, $\theta$ (see Figure 3.2 and Appendix A for the calculation of $\theta$). Likewise, the axial stiffness (A.S) was evaluated as the ratio of applied axial force to the relative axial displacement (see Appendix A) in the same region. The former is in units of newton millimeter per degree (N-m/°), while the latter is in (N/mm).

## 3.2. STUDY 2: HOW SHOULD COMPUTATIONAL SET-UP BE SUCH THAT PRE-CLINICAL TESTING OF THESE DEVICES BE PERFORMED TO OBTAIN A PHYSIOLOGICALLY ACCURATE MECHANICAL RESPONSE?

### 3.2.1. Finite Element Model Considerations

In this second part of the thesis, standardized femur model proposed by Viceconti *et al.* [60] was used, and modeling was done in ADINA 8.7.5 [61]. The reasons why we have changed the bone model for FEA and the software are explained as follows: There are several FEA studies which utilize different femur models. This situation makes it difficult to compare outputs of different studies. After we saw that some papers--interested in finding strain distribution in the femur, e.g. [31, 32]--used the standardized model in their studies. We thought that it would be more appropriate to use this bone model for the purpose of comparing our results with these studies. The change of the software is basically due to the less solution times of the static analyses provided by ADINA. In order to reduce computational effort, cancellous portion of the bone was removed. A retrograde nail-bone construct with three interlocking pins--two of which were located at proximal, and one at the distal side--was

Table 3.2. Mechanical properties of all the constituents of the bone-implant construct model [65, 31]

| Region | Elastic Modulus, $E$ (GPa) | Poisson's Ratio, $\nu$ |
|---|---|---|
| Nail (316L steel) | 200 | 0.33 |
| Bone (cortical) | 17 | 0.3 |

created. A diaphyseal osteotomy, of 5 mm was performed in the mid-diaphysis to simulate a transverse fracture. The solid nail and pins had a diameter of 11 and 4.5 mm, respectively.

Finite element analysis (FEA) enables to examine the mechanical behavior of biomedical devices [5, 6, 46, 51, 62]. When creating finite element model of the construct, several contact regions were considered which are shown in Figure 3.5 [63, 64]. Tied contact was utilized at two contact interfaces, bone to pins (b/p), and nail to pins (n/p). The interaction between medullary canal of the bone and nail (b/n) was such that frictionless sliding of the nail inside the canal was possible. The nail and pins were made of 316L grade steel. All materials were assumed to be isotropic and linearly elastic. Material properties are shown in Table 3.2. (Material properties of the bone were changed just to compare our results with a similar study in the corresponding result section). Meshes largely constituted of tetrahedral elements, the remaining parts being hexahedrals. Both first and second order elements were tested. The maximum element lengths used for the bone, nail and pins were 2, 1 and 1 mm, respectively. Mesh refinements were applied at hole locations. Bone-implant construct (BIC) was discretized by a total of 365811 elements (81933 nodes), whereas intact bone by 134738 elements (30885 nodes). The meshed view of the construct is depicted in Figure 3.5.

## 3.2.2. Boundary and Loading Conditions

The mechanical behavior of femoral constructs highly depends on the boundary and loading circumstances assigned in pre-clinical testing. It was shown that unrealistic constraints on the femur yielded excessive femoral deformations [31, 44], which necessitated simulating *in vivo* conditions by more physiologically-based boundary conditions and loads. It was seen that studies that used realistic constraints on the intact bone (e.g. [31]), in comparison with previous studies that did not do so (e.g., [29, 30]) resulted in a more physiologically accurate mechanical representation. We adapted the method proposed by Speirs *et al*. [31]
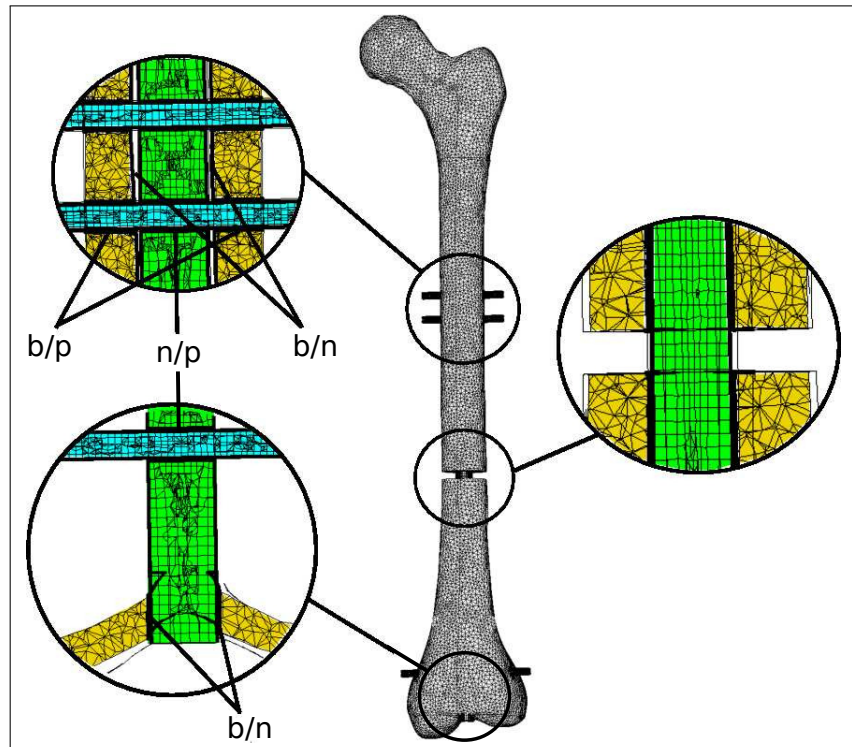
Figure 3.5. Meshed view of the bone-implant construct with section views of the contact regions, i.e., b/p: bone to pin, n/p: nail to pin and b/n: bone to nail

to analyze the mechanics of the bone-implant construct. For the purpose of comparison, two other cases of commonly used boundary and loading configurations are also tested. The three cases looked in this study are shown in Figure 3.6.

In cases (*a*) and (*b*), femur was fully-constrained at its distal condyles as it was done in previous studies [28, 29]. However, in case (*c*), femur was only constrained at two points simulating a more realistic knee contact, reflecting a more physiologically accurate condition [31]. In addition, the hip joint (point *Q*) was only allowed to translate along an axis from the femoral head to the knee center (local $x_l$ axis defined at point *Q* between points *Q* and *O*). To prevent rigid body motion, a node at the knee center was restricted in three translational degrees of freedom ($x$, $y$, $z$); and anterior-posterior (A-P) motion ($y$) of a point *N*, at the distal lateral (L) epicondyle was also constrained.

When it comes to loading, case (*a*) utilizes only a hip contact force at point *X*, whereas additionally reduced muscle loading together with the hip contact force [43], in cases (*b*) and (*c*). Instead of including all muscles and joint forces in the numeric models [31, 32],
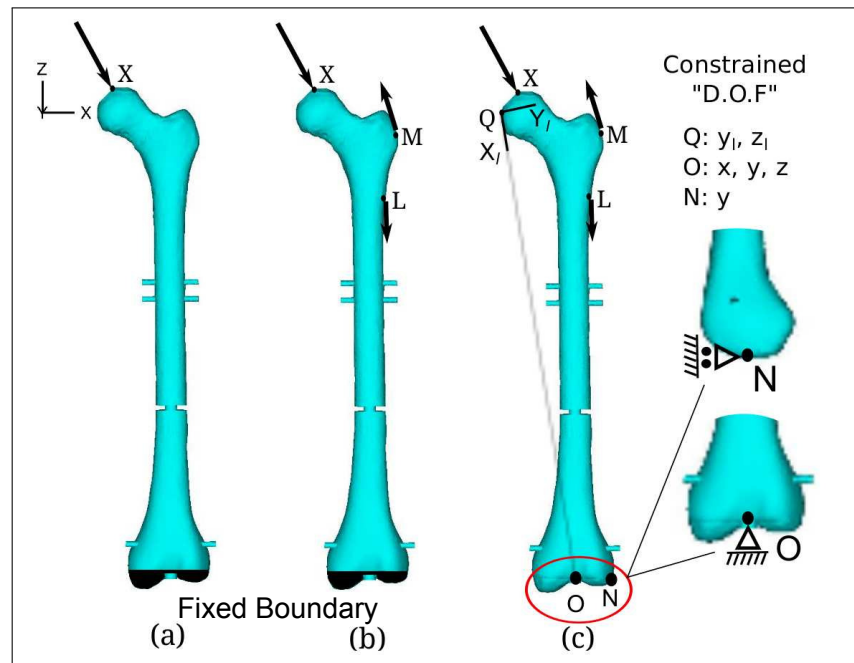
Figure 3.6. Boundary and loading conditions considered in this study: Case (*a*) consists of hip contact force with fixed boundary conditions on the distal condyles. Case (*b*) is the same as (*a*), but including additional muscle forces (abductor, tensor fascia latae and vastus lateralis). Case (*c*) corresponds to physiological conditions with joint constraints

Table 3.3. Load profile of the bone-implant construct and the intact bone at the instant of maximum hip contact force during the gait cycle (BW=860 N) [43]

| Force (N) | $x$ | $y$ | $z$ | Point |
|---|---|---|---|---|
| hip contact | 464.4 | 282.1 | -1971.1 | X |
| abductor | -498.8 | -37.0 | 743.9 | M |
| tensor fascia latae, proximal part | -61.9 | -99.8 | 113.5 | M |
| tensor fascia latae, distal part | 4.3 | 6.0 | -163.4 | M |
| vastus lateralis | 7.7 | -159.1 | -798.9 | L |

some muscles which showed no or negligible effect during walking were excluded. The loading model--comprising of hip contact, abductor, tensor fascia latae (proximal and distal parts) and vastus lateralis forces--provided a realistic approximation of physiological loading conditions (L.C), and seems achievable in *in vitro* test set-ups according to Heller *et al*. [43]. In all cases, maximum hip contact force of the gait cycle in walking was used for loading. The magnitude and point of applications of these loads were approximated for the standardized femur model, for a patient of 860 N body weight (BW), and given in Table 3.3. Note that load applied at point *M* is the resultant of the abductor and tensor fascia latae forces.

### 3.2.3. Mesh Sensitivity Analysis

A mesh sensitivity analysis is the key to ensure a reliability of the finite element model, yet are usually overlooked in biomechanical studies [66]. In analyzing complex structures, e.g., bone, ``some researchers have focused on the development of improved geometric precision, whereas others have focused on improved representations of the material behavior [67]. Another factor which intrinsically affect the results of an FEA study is the mesh quality. In order to reach accurate models, finite element mesh should be sufficiently refined [66,68]. Therefore, with regard to models' accuracy, we conducted a mesh sensitivity analysis for the intact bone with two types of standard tetrahedral elements (4-node linear and 10-node quadratic) by changing the total number of degrees of freedom (NDOF) in the model.

# 4. RESULTS

## 4.1. STUDY 1

Several ANSYS runs were performed, for different geometries, loads, and fit types. The outcomes were organized in three groups in relation to: 1) load transfer, 2) constructs' stiffness, and 3) contact forces.
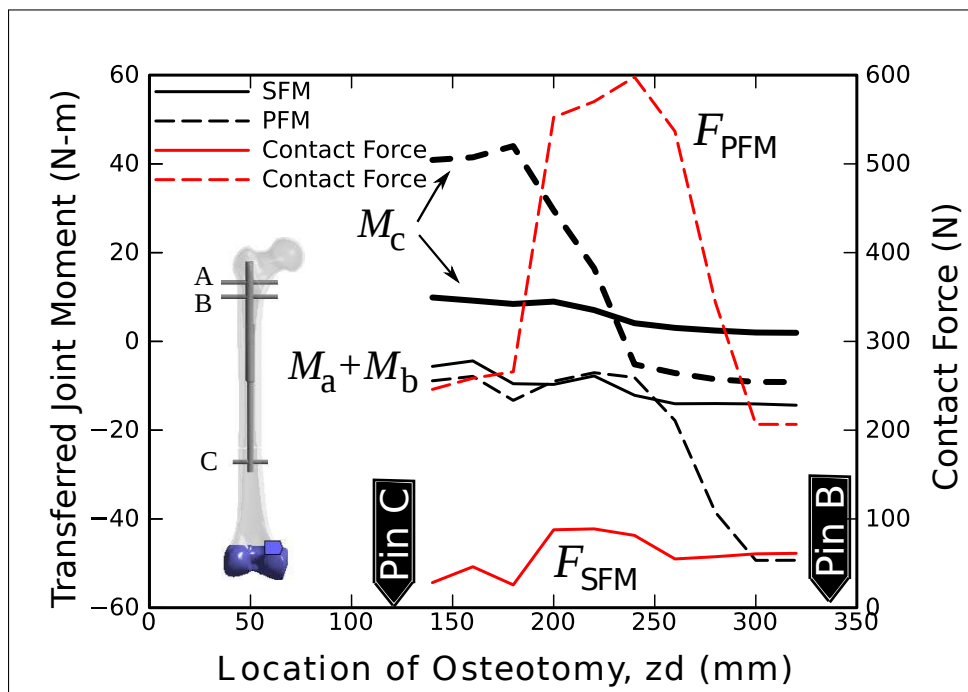


Figure 4.1. Transferred joint moment distribution versus location-of-osteotomy, for antegrade-type fit under SFM and PFM. Red curves $F_{PFM}$ and $F_{SFM}$ represent the contact force as a result of PFM (dashed) and SFM (solid) cases, respectively

Firstly, comparative graphs depicting the mediolateral moments transferred between the bone and the nail as a function of the location-of-osteotomy are presented in Figures 4.1 and 4.2 for antegrade and retrograde type fits, respectively. Here, solid-bold lines were used to represent the spring-force model (SFM), while the dashed-bold lines did the point-force model (PFM). The nail was fitted in the antegrade configuration in Figure 4.1, while it was in retrograde configuration in Figure 4.2. For antegrade-type fits, the location-of-osteotomy varied between pins $B$ and $C$, where $M_c$ and $M_a + M_b$ indicate the moment transmitted

by pin $C$ and the summation of those by pins $A$ and $B$, respectively (see Figure 3.3). For retrograde-type fits, location-of-osteotomy varied between pins $E$ and $F$. Additionally, the contact forces normal to the bone-nail interface are plotted along with others in Figs. 4.1 and 4.2, where the solid red curve depicts the SFM and the dashed red one does the PFM.
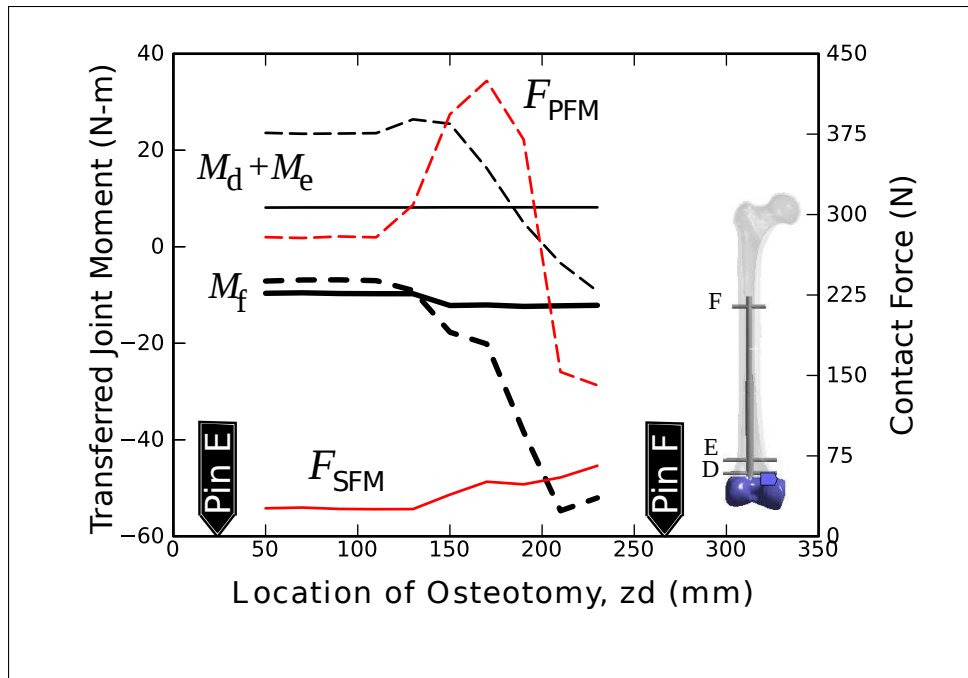


Figure 4.2. Transferred joint moment distribution versus location-of-osteotomy, for retrograde-type fit under SFM and PFM. Red curves $F_{PFM}$ and $F_{SFM}$ represent the contact force as a result of PFM (dashed) and SFM (solid) cases, respectively

Next, the contribution of an additional pin at a joint location was investigated as a function of location-of-osteotomy in Figure 4.3, corresponding to the antegrade(top), and retrograde-type (bottom) fits under SFM, respectively. While the light gray curves $M_a$ and $M_b$ in this figure depict the moments transmitted by pins $A$ and $B$, respectively; their summation--the solid-bold line $M_a + M_b$--depicts the total moment transmitted at the proximal segment. The dashed-bold line (curve $M_c$), depicts the moment transmitted by pin $C$ in the distal segment. Note that the two curves are roughly offset at a distance $M_1$. The situation for a retrograde-type fitting is shown in the bottom of Figure 4.3. Light gray curves $M_d$ and $M_e$--moments transmitted by pins $D$ and $E$, respectively--were summed in the solid-bold curve $M_d + M_e$ reflecting the total moment transmitted at the distal segment. The dashed-bold line (curve $M_f$) indicates the moment transmitted by pin $F$ in the proximal segment.
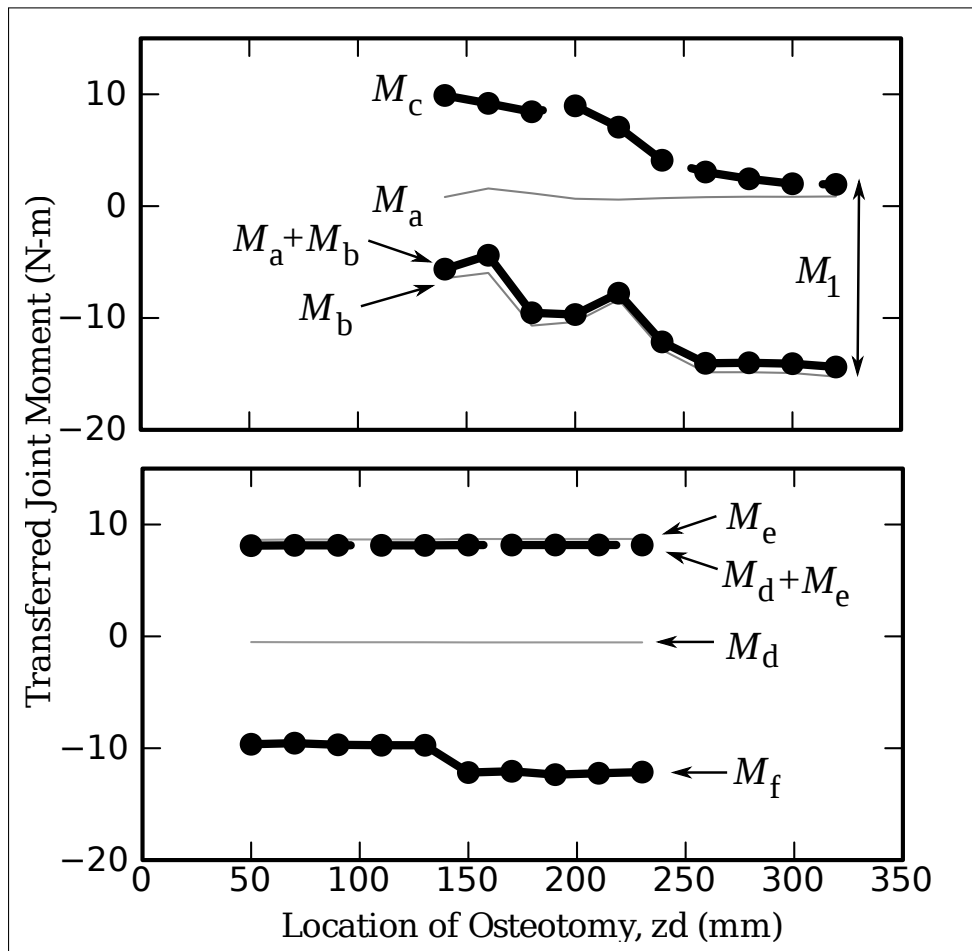
Figure 4.3. Top: Transferred joint moment distribution versus location-of-osteotomy, for an antegrade-type fit under SFM. Bottom: same for a retrograde-type fit. The solid circles depict actual data points

As a by-product of the current study, stiffness values in two modes (axial and bending) were extracted from the numerical results as described at the end of 3.1.3. In Figure 4.4, axial and bending stiffness were combined for antegrade and retrograde-type fits. In this graph, solid curves depict the variation of stiffness versus location-of-osteotomy, corresponding to each fitting configurations. The solid-bold curves (to the right) correspond to antegrade-type fit, while the dashed ones to retrograde-type fit.
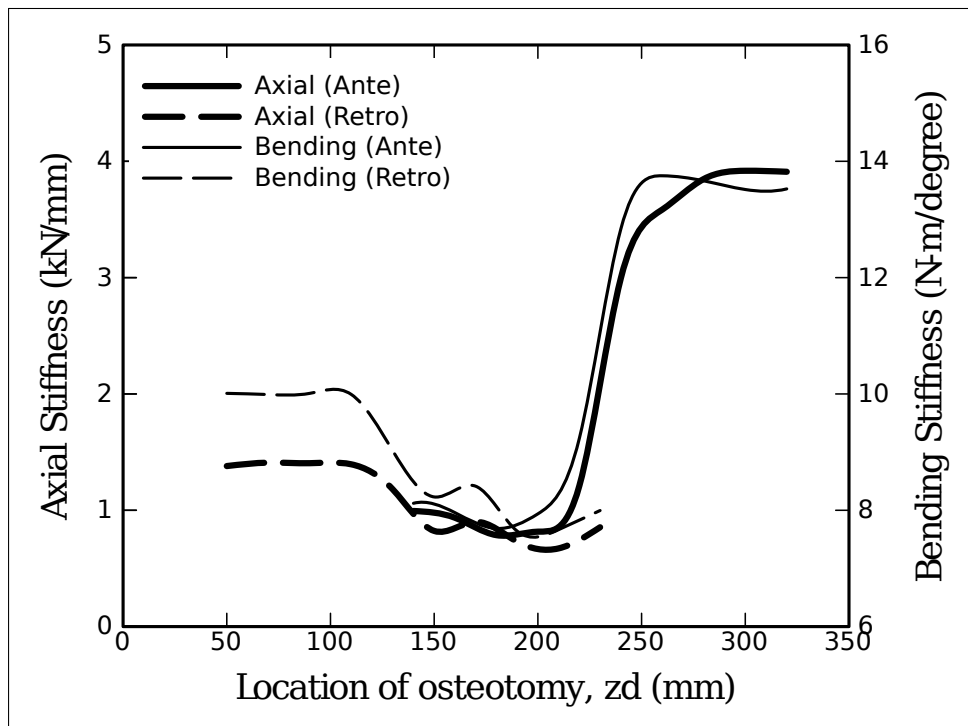


Figure 4.4. Variation of axial and bending stiffness as a function of location-of-osteotomy, $z_D$, for antegrade- and retrograde-type fits under PFM and pure bending moment, respectively

## 4.2. STUDY 2

### 4.2.1. Mesh Sensitivity Analysis

Results are illustrated based on the error of the hip displacement. Error for $h-$refinement with respect to the linear and quadratic elements is found by the equation below.

$$E^J = \frac{\|U_Q^T - U_Q^J\|}{\|U_Q^T\|} \tag{4.1}$$

In this equation, $U_Q^T$ represents the reference displacement in the local $X_L$ direction at point $Q$ (see Figure 3.6) obtained using a mesh of 872895 NDOF quadratic elements. Calculated errors for $U_Q^J$ indicate trial meshes where $J = 1, 2, 3, 4$ correspond to 1512, 5274, 23217, 124989 NDOF in the linear elements' case, and $J = 5, 6, 7$ to 9108, 32259, 150090 in the quadratic case; respectively. Convergence behaviors of two types of elements with different orders (i.e., linear and quadratic) is portrayed in Figure 4.5. In this figure, error is plotted as a function of the number of degrees of freedom used in the models. Quadratic tetrahedral elements provide faster convergence than linear elements do, according to the calculations. Based on the sensitivity analysis, it is seen that our results using 2 mm linear elements are accurate to within a relative percent error of about 18 %.
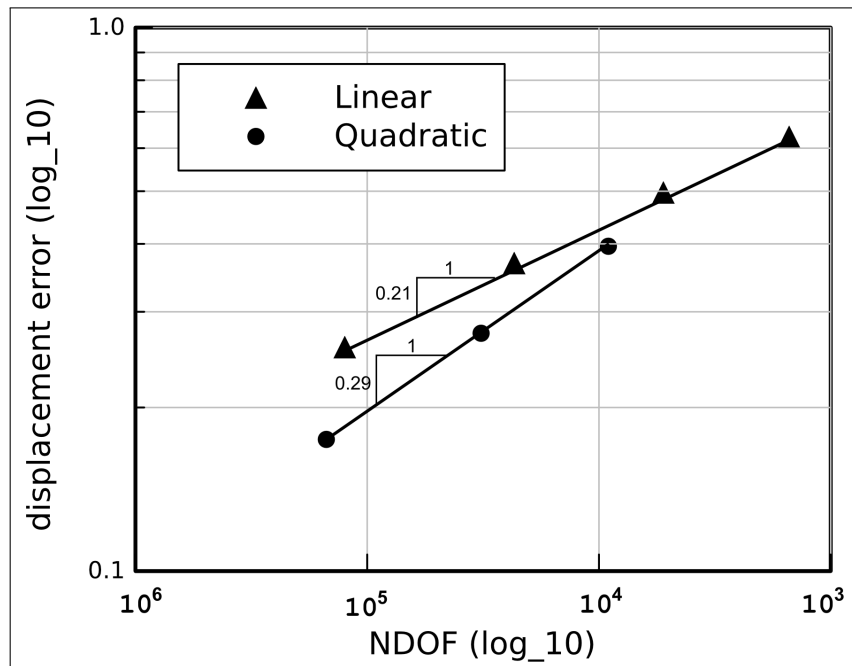
Figure 4.5. Mesh sensitivity analysis with respect to number of degrees of freedom using 4-node linear and 10-node quadratic tetrahedral elements

### 4.2.2. Femoral Displacements

Deflected constructs in the medial (M) and anterior (A) views compared to undeflected shapes are shown in Figure 4.6, for three boundary and loading configurations. It is not suprising to see that the application of hip contact force alone produced significant bending in A-P and M-L planes, resulting a total displacement magnitude above 20 mm at the femoral head (top) in case ($a$). However, addition of muscle forces--abductor, tensor fascia latae and vastus lateralis--seems to prevent excessive bending in the sagittal plane caused by hip contact force ($2^{nd}$ row), but increasing the deflection of the construct to a magnitude of nearly 24 mm in the coronal plane. The displacement of the construct gets smaller when the joint constraints are imposed ($3^{rd}$ row), balancing bending in the coronal plane, (see Figure 3.6). In case ($c$), maximum displacements are read around 7 mm at the greater trochanter and it is 3.5 mm in the shaft region of the construct. Displacement of the intact bone under case ($c$) is also plotted at the bottom of the same figure. Maximum value of displacement is read as 2.5 mm for the intact femur in the mid-shaft region, whereas it is around 1.5 mm at femoral head.
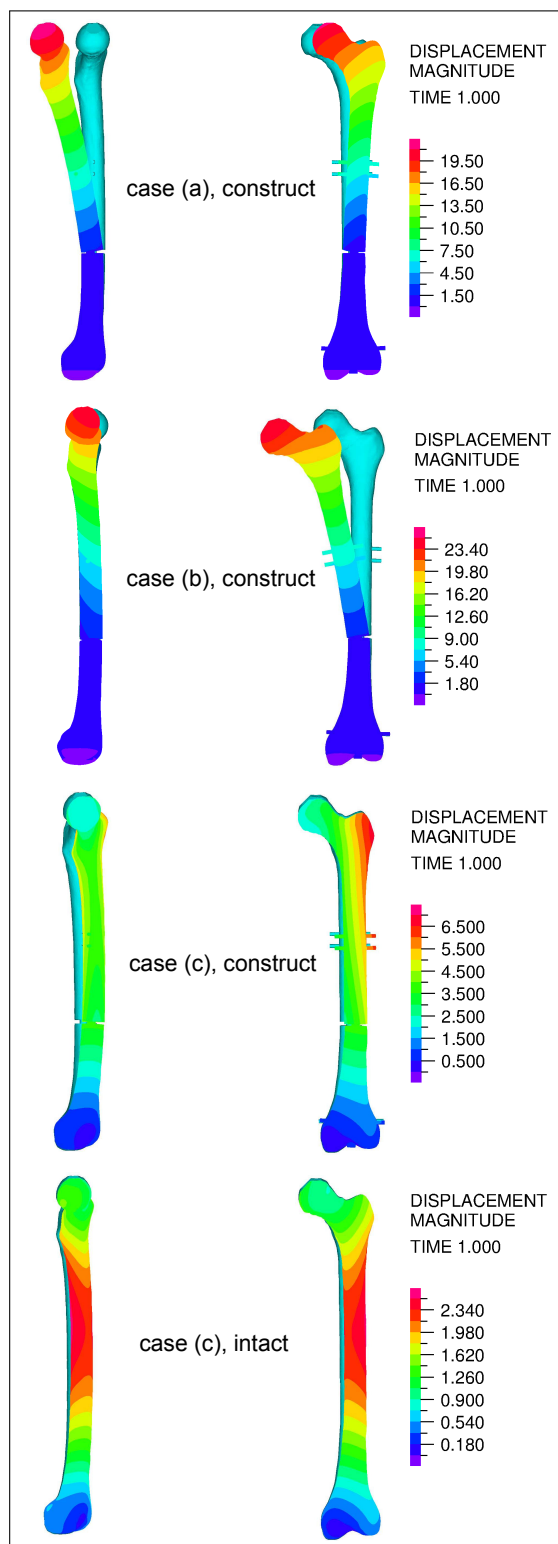
Figure 4.6. Displacement distributions on the bone-implant construct and intact bone under walking loads for three boundary and loading configurations in the medial (left) and anterior (right) views. Top: case (*a*), $2^{nd}$ row: case (*b*), $3^{rd}$ row: case (*c*) and bottom: case (*c*) intact. Displacements are exaggerated 3x for clarity

### 4.2.3. Principal Strain Distributions

Principal strain distributions along the A-P (left column) and M-L (right column) sides of the implanted-femur cortex (black circles) and outer nail surface (red circles) are depicted for cases (*a*), (*b*) and (*c*) in the first three rows of Figure 4.7; whereas those for the intact femur is plotted in the last row. Localized strain ascensions occur in the bone where concentrated muscle forces are applied. Strains also increase around the regions of interlocking pin holes where load transfer from bone to nail and *vice versa* occurs. For the bone cortex in general, principal strains on the M-L sides are higher than those on the A-P sides; and those in the coronal plane are higher in comparison with the sagittal plane except maybe for case (*a*). From the strain distribution in the intact bone (depicted at the bottom of the Figure 4.7), the peak strain in the coronal plane is read on the medial side as -2500 $\mu\epsilon$, while in the sagittal plane it is read on the posterior side as 1000 $\mu\epsilon$.

In the nails, peak values of principal strains are always at the fracture site. Peak values on posterior (-3500 $\mu\epsilon$) and anterior (3500 $\mu\epsilon$) sides are much higher than those on the medial (-500 $\mu\epsilon$) and lateral (500 $\mu\epsilon$) sides in case (*a*). However, the situation is reversed in cases (*b*) and (*c*) where strains in the coronal plane are much higher than those in the sagittal plane. In case (*b*) the peak principal strain goes superficially as high as -5000 $\mu\epsilon$ and 4500 $\mu\epsilon$ on the medial and lateral edges, respectively; while in case (*c*), it is around -2500 $\mu\epsilon$ on the medial side, and 2500 $\mu\epsilon$ on the lateral side. It is important to note the two-fold difference in peak nail strains between cases (b) and (c).

### 4.2.4. Reaction and Contact Forces

Reaction forces that arise in bone-implant construct under walking loads are given in Table 4.1. Reaction components for cases (*a*) and (*b*) correspond to the summation of all those nodes constrained at the distal side of the femur. For case (*c*), reactions are reported for the three constrained joints, i.e., points *N*, *Q* and *O*. At the knee, in the *z*-axis, a reaction of 2076 N occurs in case (*b*). Due to the constraint at the femoral head (point *Q*), a reaction of 280 N is obtained in the M-L direction. Reaction components for case (*c*) were validated against an equilibrium analysis of a similar structure. In Figure 4.8, contact force distribution between the retrograde nail, and the proximal and distal sides of the femur for three boundary
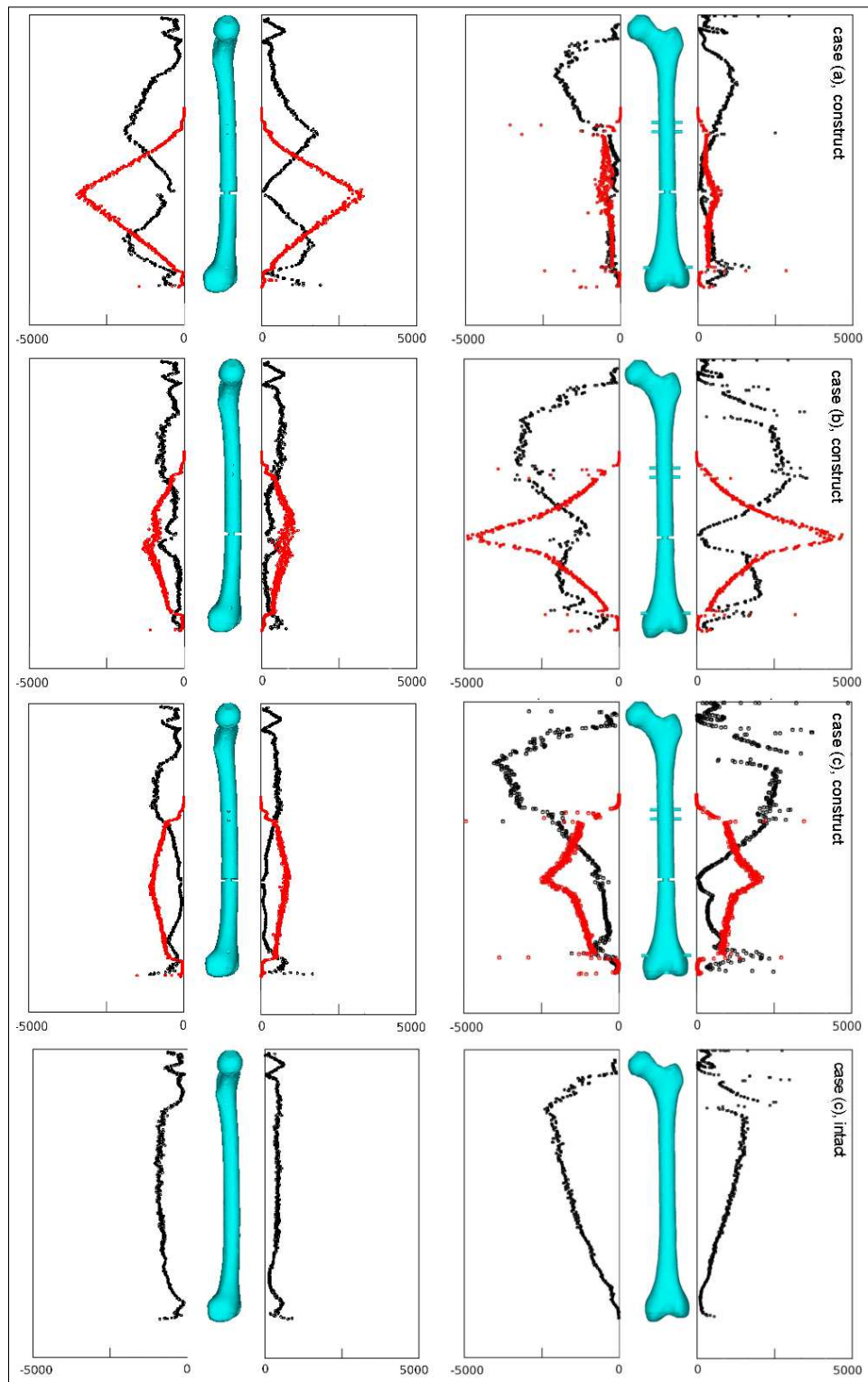
Figure 4.7. Main principal strain distributions (in $\mu\epsilon$) on the cortex of the bone (black circles), in the nail (red circles) and intact bone under walking loads for three cases. Left: posterior and anterior sides, right: medial and lateral sides. Top: case (*a*), $2^{nd}$ row: case (*b*), $3^{rd}$ row: case (*c*) and bottom: case (*c*) intact

Table 4.1. Reaction force magnitudes at the support regions of the constructs' under walking loads

| Case | Support | $x$ | $y$ | $z$ |
|------|---------|-----|-----|-----|
| (a) | Distal condyle | -464 | -282 | 1971 |
| (b) | Distal condyle | 84 | 8 | 2076 |
| (c) | $N$ | 0 | 590 | 0 |
|  | $Q$ | 278 | 6 | 42 |
|  | $O$ | -194 | -588 | 2034 |

and loading configurations is depicted. It is clear from the figure that application of different boundary and loading conditions altered the contact regions as well as their magnitudes. A superficial contact force of 2400 N is measured on the medial side of the nail at the close proximity of the fracture site (region $k$) in case ($b$). In general, lower values of contact forces are seen towards proximal and distal ends of the nail in comparison with the fracture-site.
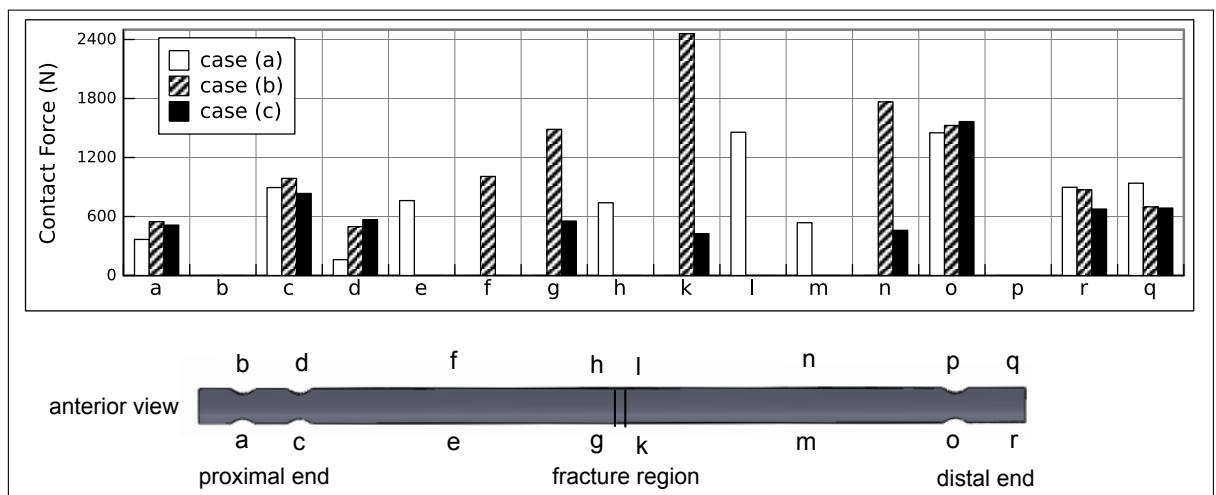


Figure 4.8. Contact forces at the several regions of the nail by the femur

# 5. DISCUSSION

## 5.1. STUDY 1

Based on the results in Section 4.1, we attempted to shed light onto the effect of loading type on the moments transferred at the interlocking pins. In addition, implant safety was discussed. Finally, the results obtained for stiffness variation were reported and compared with previous findings in similar studies.

### 5.1.1. Moments Transferred at the Interlocking Pins

The interlocking pins have the primary functions of transmitting loads between and providing for the stability of the bone/nail construct. It is especially interesting to study the moment transfers, as these are thought to be the main cause of mechanical failure of these parts. Note that the IM nail contains only one interlocking pin in the moving (telescopic) part, while two adjacent ones at the stationary side. Firstly, the change of mediolateral bending moments transmitted at the interlocking pins is investigated as a function of the location-of-osteotomy. At the top of Figure 4.3 (SFM, antegrade), changing osteotomy location from the distal side towards the proximal leads to a drop in $M_c$ from 10 N-m to around zero, while the sum $M_a + M_b$ drops from -5 to -15 N-m. The situation for the retrograde-type fit shown in bottom of the same figure is slightly different, depicting virtually constant moments, for both the distal ($\approx$ 7.5 N-m) and proximal ($\approx$ -10 N-m) pins.

Interestingly, loads were not shared equally by the adjacent pin pairs ($A$ and $B$ in the antegrade and, $D$ and $E$ in the retrograde-type fits), as seen in figure 4.3. The pins closer to the osteotomy site ($B$ in the antegrade and $E$ in the retrograde fits) transmitted a significant portion of the moment, while their neighbors beared nearly zero load. Thus, including an additional pin at a connection does not significantly affect the moment transmitted by a single pin during lengthening.

Looking at the results between SFM and PFM in Figures 4.1 and 4.2, it was seen that the transmitted moment magnitudes were significantly different for the two cases. The moment

values in SFM remained well-below those predicted by PFM. We therefore assert that PFM based designs would lead to an implant with excessively conservative dimensions. SFM is a more realistic representation of the loading during the lengthening phase, and thus should be included in the life cycle design analysis of the implant along with PFM.

## 5.1.2. Stiffness of the Construct

Qualitatively, curves for the axial and bending stiffnesses are astonishingly close. The fit-type does not seem to have any appreciable effect on either of the stiffnesses. This is reflected in the smooth transition from retrograde-type to antegrade-type fit in Figure 4.4 as one traverses from the lower-distal end fracture ($z_D = 50$), passing the mid-shaft fracture zone, and ending in the proximal-fracture zone. Moreover, a depression is observed in both axial and bending stiffnesses in the mid-shaft osteotomy zone. This is attributed to the change in contact behavior as the osteotomy enters the mid-shaft region.

In an attempt to validate our results, three studies involving intramedullary nails used for fracture fixation were identified (Schandelmaier et al. [30], Chen et al. [6], and Penzkofer et al. [14]). In all the above references axial stiffnesses were obtained by loading the model axially from the hip-joint, and thus we compared their findings with our PFM results. The bending stiffness presented in [30] was found by loading the construct in pure bending and so did we. The values are presented in Table 5.1.

In general, stiffness values are in good agreement with each other. It is important to note that, reamed cadaver femur and unreamed cadaver tibia were tested, in [30] and [14], respectively, under mid-shaft osteotomy condition; whereas, in [6], a reamed composite femur was tested under lower-distal osteotomy condition. Thus, the first set of comparisons, including [6] and *Present Study*[1], looks at the lower-distal osteotomy zone; while the second set, including *Present Study*[2] and the others, looks at the mid-shaft osteotomy. The nails in the previous studies were, a solid 9 mm one in [30], a hollow 13.5/5.4 mm (OD/ID) nail in [6], and two different solid nails of 9 and 11 mm in [14]. The nail and bone were locked by 3 distal and 2 proximal pins in [14] and [6], while only one pin per each side was used in [30]. Locking-pins were of size 4.3-4.9 mm in [30].

Table 5.1. Two sets of comparative stiffness reports, first with Chen [6], and then with [14] and [30]. *Present Study*[1]: Results for lower-distal fracture with retrograde-type fit. *Present Study*[2]: Results for mid-shaft fracture with antegrade-type fit

| Studies | Axial | Bending |
|---|---|---|
| Chen *et al.*, [6] | $1.58 \pm .05$ | - |
| **Present Study**[1] | | |
| *PFM* | $1.4$ | - |
| *Pure Bending* | - | $10$ |
| Penzkofer *et al.*, [14] | | |
| 9 mm nail | $0.72 \pm .42$ | - |
| 11 mm nail | $1.04 \pm .30$ | - |
| Schandelmaier *et al.*, [30] | $1.75 \pm .14$ | $7.05 \pm 0.2$ |
| **Present Study**[2] | | |
| *PFM* | $0.82 - 0.99$ | - |
| *Pure Bending* | - | $7.7 - 8.1$ |

### 5.1.3. Contact Forces

The contact forces that arise in the SFM are much lower in magnitude than those in the PFM, for both antegrade- and retrograde-type fits. This is mainly due to the eccentricity of the in the PFM. In antegrade-type fits, PFM contact force exceeds half the total applied load for the range of osteotomy locations $190 < z_d < 260$, attaining a maximum of 600 N around the midpoint between pins $B$ and $C$. In retrograde-type fits, a peak in the PFM contact force is observed between pins $E$ and $F$, but its magnitude remains below half the total applied load in the entire range, attaining a peak of 410 N. The SFM contact forces are below one-tenth the applied load, for both retrograde- and antegrade-type fits.

The arisal of normal contact force results in partial load-sharing between the nail and the unloaded portion of the femur, which, in turn prevents stress shielding. Note that, in all finite element analyses the nail was allowed to slide without friction in the IM canal, while normal contact forces were used to restrict penetration at the nail/bone interface. We anticipate that frictional effects do not play a major role in the distribution or magnitude of mediolateral moments due to their small eccentricity from the anatomical axis. Validation of frictional forces was not possible as there were no known references to compare with.

The finite element results illustrate that actual contact conditions during lengthening (SFM)

may not be as severe as the *in vitro* predictions (PFM). Furthermore, as seen from the PFM results (simulating *in vitro* conditions), when the osteotomy is around the midpoint between the two pin connections ($B$ and $C$ in the antegrade-, $E$ and $F$ in the retrograde-type fits) contact force becomes a maximum. Thus, in order to avoid high contact stresses between the nail and the bone segments, it is advisable to keep the osteotomy away from the mid-range between the pin connections.

## 5.2. STUDY 2

Pre-clinical testing of IM nails is critical to determine stability and performance targets for these devices. Understanding the *in vivo* conditions which these devices operate under, carries a primary importance in this regard. However, there is still lack of consensus on the boundary and loading conditions to apply in these tests. According to Bergmann *et al*. [26], femoral implants should mainly be tested under walking and stair climbing loads, as these activities resulted in the most critical loading of the femur. This hypothesis is further supported by the work of Morlock *et al*. [27], which showed walking to be the most frequent dynamic activity of a total hip arthroplasty (THR) patient. In the literature, several boundary and loading conditions were employed in either experimental tests [28, 29] or numerical models [29, 31, 32] in an attempt to investigate the mechanical behavior of the implanted or intact bone. Because there is no standard accepted procedure of applying boundary and loading conditions in these tests, results show huge variations which makes it difficult to compare outputs of different studies.

### 5.2.1. Model Verification in the Light of Previous in vivo and Numerical Studies

Unfortunately, to the knowledge of the authors', there is no *in vivo* study of an retrograde nail-implanted femur during walking. Therefore, numerical model of the intact bone corresponding to case($c$) will be compared with similar studies in the literature. In this study, displacements and main principal strain distributions of the intact bone are presented at the bottom of Figs. 4.6 and 4.7, respectively. Principal strains showed resemblance with the results given by Duda *et al*. [32]. Their study included all thigh muscles of the gait where distal end of the bone was restricted in translation at three points. Speirs *et al*. [31] presented main principal strains on the intact bone applying physiological constraints for the instant of maximum hip contact force during the gait cycle. For only comparison purpose, an extra figure has been created. The comparison of principal strain distribution is depicted in Figure 5.1.

Strain distribution in the intact bone in Figure 4.7 is in agreement both qualitatively and quantitatively with [31] along all surfaces, with the only exception of a slight underestimate of their results in the sagittal plane. In both studies, peak strains are seen in the subtrochanteric
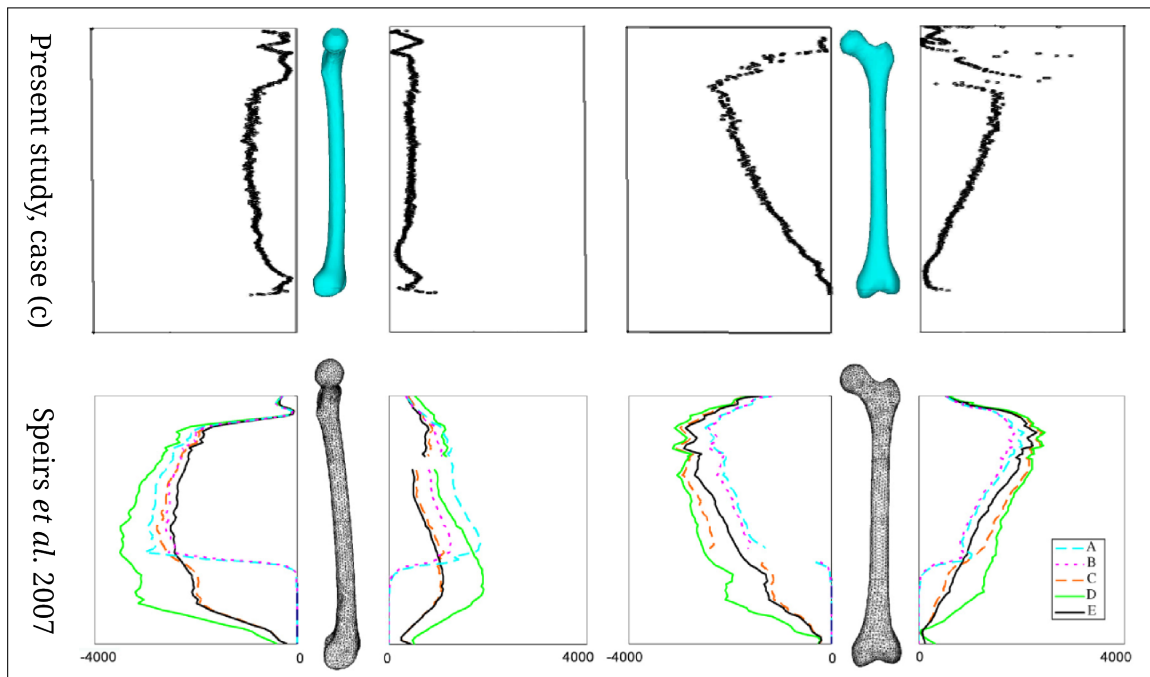
Figure 5.1. Comparison of main principal strain distributions in the intact bone with the study [31]

region along the M-L sides, while they are in the mid-diaphysis on the A-P sides. Note that their study included a very complex loading model that comprised of joint contact forces (hip, knee and patella) as well as all muscles, contrary to our study which utilized hip contact force and reduced muscle forces (abductor, tensor fascia latae and vastus lateralis) proposed by Heller *et al*. [43]. Unfortunately, magnitudes of the joint and muscle forces applied in [31] was not presented. Thus, it can only be assumed that the slight underestimation of strains in the sagittal plane is caused by the complex loading factor. Finally, as an accuracy indicator, the reduced muscle loading model proposed by [43] and used in this study has been reported to predict the *in vivo* hip contact force [26] with an error of 7%. However, the complex loading model used in the study of Speirs *et al*. [31] was reported to predict the *in vivo* hip contact forces by an error of 12%.

An interesting study utilizing linear and non-linear implementations of a free boundary condition modeling on the femur by Phillips [69], reported the principal strains in the femur and deflection of the femoral head in one-legged stance position. Strains and displacement of the femoral head presented in our study are consistent with his findings. Displacement distribution of the intact femur shown in Figure 4.6 compares well with the results of another

*in vivo* study by Taylor *et al*. [44], where radiological measurement of the femoral head displacement in one-legged stance position was performed. There, it was stated that the femur is primarily under compression loading, similar to our case (*c*).

Including all muscles in an experimental set-up or finite element analysis is a complex process making the controllability and reproducibility of tests difficult. From engineering point of view, we conclude that the reduced muscle loading model proposed in [43], along with the joint constraints proposed in [31] are adequate for a physiologically accurate mechanical representation of a nail-bone construct.

### 5.2.2.  Principal Strain Distributions in the Construct

The application of hip contact force alone was shown to be an oversimplified loading situation resulting in huge deflections in the femur due to bending [28, 45], and therefore resulted in unrealistic straining of the femur. This is readily seen from Figure 4.7 where higher strain magnitudes are observed on the A-P side compared to the M-L side in case (*a*), while the reverse is true for case (*b*), i.e., strain magnitudes are higher on the M-L side compared with the A-P side. This is mainly a result of including the reduced muscle loading model in case (*b*) which, in turn, results in a reduced bending moment in the sagittal plane, while the bending moment in the coronal plane is reversed. The main difference in terms of strain distributions between cases (*b*) and (*c*) are observed in the two-fold decrease of peak strain magnitudes in the coronal plane for the nail in case (*c*). This is attributed to the inclusion of joint constraints in case (*c*) which acts to balance the bending effect in the coronal plane.

Not surprisingly, peak values of strain in the nails are observed at the fracture site. This is because of the contact load that arises in the nail at the fracture site. During fracture healing, the forces in the nail decrease while they are increasing in the bone. However, it is reported by Schneider *et al*. [21] that even after fracture consolidation, a nail carries up to 50% of the initial external loads. In another study [1], it is stated that ``In cases of non-union or mal-union of the bone fragments, the nail can be subjected to an excessive portion of the external load at full weight-bearing instances, which can promotes short-term fatigue fracture of the nail''. In that study, several case studies of interlocking nails in which nail failures were observed at the fracture site due to large plastic strain was also reported. Thus, the accurate estimate of peak strains as given in case (*c*) in Figure 4.7 becomes even more important in the design of nails against failure.

### 5.2.3. Reaction and Contact Forces

Correct identification of forces that arise in a bone-nail construct should carry significance in the eye of a designer. Apart from the joint-muscle loads, the nail is also exposed to contact forces due to the interaction between the bone and the nail, at the interlocking pin locations as well as the fracture site. In order to shed light on the rather complex bone-nail contact interaction, and the effect of load cases on this interaction, we used Figure 4.8 which depicts contact forces grouped at several regions of the contact surface. In general, the contact forces encountered in mid-regions of the nail (*f, g, k, l* and *n*) are higher compared to proximal and distal regions, for all load cases. Superficial contact forces arose in cases (*a*) and (*b*) in the mid-shaft region, which is an indication of the excessive bending moments in these cases. The contact force magnitudes in case (*c*) are observed to be relatively lower in general.

The reaction forces presented in Figure 4.1 are all seen to be in agreement with a simple statics equilibrium model, i.e., the sum of external forces is equal to the sum of reactions. Restriction of the point *Q* at the femoral head results in the arisal of a so-called *residual reaction* force of 280 N at this location (the term residual is used to indicate that this force is in excess of the measured hip-joint contact force). This residual reaction is labeled to be non-physiological by some authors, as it has been stated in the letter of Paul [70] regarding the study of Simoes *et al*. [28], where a similar reaction force at femoral head as a result of the constraining the head motion in horizontal direction was reported. It is worth mentioning that the constraining of the femur left the structure as one of a statically-indeterminate type

in [28], whereas that is not the case in our study. While it is true that the *in vivo* measurements of the hip contact force should account for all the forces arising at the hip joint, we still need the addition of this constraint in order to make our model more physiologically accurate. This reaction is certainly caused by the imbalance of externally applied (muscle and joint) forces in the model. Until more accurate data regarding the magnitude and location of the muscle loads is found, it may be plausible to eliminate or minimize this residual reaction by other means such as optimization. This inevitably will be the subject of a further study.

# 6. CONCLUSION

The primary outcomes--pertaining to the lengthening phase of an intramedullary nail-bone construct system--from a series of finite element analyzes, were summarized in section 5.1. It was found, by comparing two distinct representative force-systems, that the loading model has a considerable effect on the magnitudes of the mediolateral bending moments transmitted by the construct. Moreover, constructs with distal and proximal osteotomies had higher stiffness compared to mid-shaft osteotomies. The stiffness values were, in general, in good agreement with previously reported ones validating the reliability of the finite element model. In order to avoid high contact stresses between the nail and the bone segments, it is advisable to keep the osteotomy away from the mid-range between the pin connections. It was also shown that including an additional pin did not effectively reduce the load carried by a single pin.

The finite element models of the bone-implant construct and intact bone (under walking loads) presented herewith allowed us to estimate the mechanical behavior of the implants' more accurately in the design stage as discussed in section 5.2. The effect of different boundary and loading configurations on the mechanical behavior of the construct showed that reduced muscle force model and femoral-head joint constraint are necessary to simulate *in vivo* conditions of the lower extremity more accurately. The excess force that develops at a femoral-head joint constraint is an indication of the degree of external load imbalance, and needs to be studied further.

# APPENDIX A: CALCULATION OF AXIAL AND BENDING STIFFNESS

In this part of the thesis, a methodology is presented for the calculation of stiffness values of the constructs, i.e. axial and bending. In order for stiffness calculations, axial displacement in the interval $H$-$G$ and bending angle about $y$-axis, $\theta$, at $G$ (please see Figure 3.2) are required, and found by following below procedures.

## A.1. LOCATING CENTER OF THE CROSS SECTION AT $G$ IN ITS UNDEFORMED STATE

We define three points $(P_1, P_2, P_3)$ on the cortex of the bone at section $G$, approximately equally spaced around the circumference as shown in Figure 6.1. We write the vectors $\vec{V_1}$, $\vec{V_2}$ and their unit directions as:

$$\vec{V_1} = \vec{P_1} - \vec{P_3} \tag{6.1}$$

$$\vec{V_2} = \vec{P_2} - \vec{P_3} \tag{6.2}$$

$$\vec{U_1} = \frac{\vec{V_1}}{\|\vec{V_1}\|} \tag{6.3}$$

$$\vec{U_2} = \frac{\vec{V_2}}{\|\vec{V_2}\|} \tag{6.4}$$
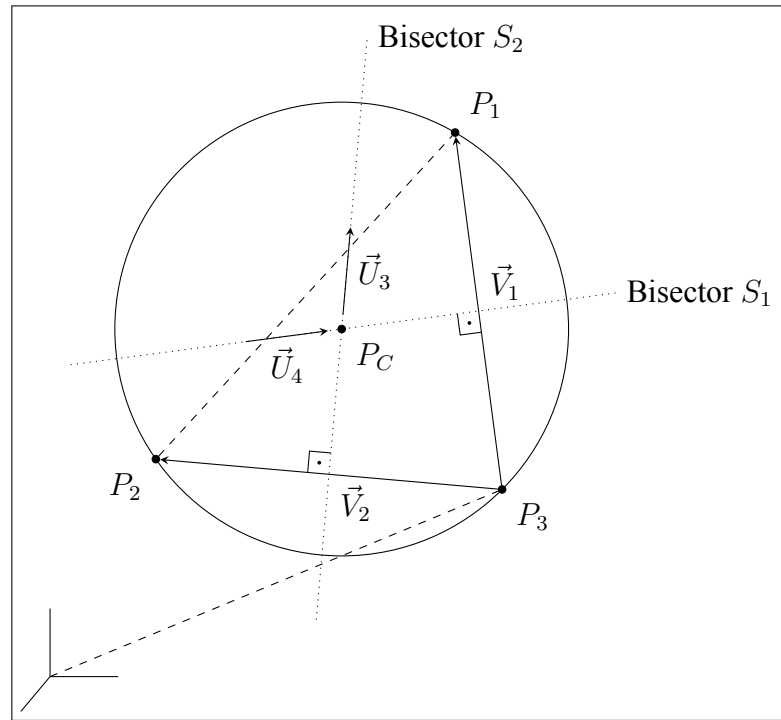
Figure 6.1. Schematic of the idealized cross section of the bone at $G$.

Outer normal of the plane defined by vectors $\vec{V_1}$ and $\vec{V_2}$, is found by taking their cross products as:

$$\overrightarrow{N_P} = \overrightarrow{U_1} \times \overrightarrow{U_2} \tag{6.5}$$

Then, unit vectors of two bisectors ($\overrightarrow{U_3}$, $\overrightarrow{U_4}$) are found by cross products of these vectors with $\overrightarrow{N_P}$ as:

$$\overrightarrow{U_3} = \overrightarrow{U_2} \times \overrightarrow{N_P} \tag{6.6}$$

$$\overrightarrow{U_4} = \overrightarrow{U_1} \times \overrightarrow{N_P} \tag{6.7}$$

The equations of the lines defining bisectors 1 and 2 are written, where $R^\star$ and $S^\star$ are parametric coordinates of circle center on vectors $\vec{U_3}$ and $\vec{U_4}$, respectively.

$$\vec{S_1} : \frac{\vec{V_1}}{2} + R^\star\vec{U_4} \tag{6.8}$$

$$\vec{S_2} : \frac{\vec{V_2}}{2} + S^\star\vec{U_3} \tag{6.9}$$

The center of the cross section at $G$ in its undeformed state is located at the intersection of the two bisectors $\vec{S_1}$ and $\vec{S_2}$:

$$\frac{\vec{V_1}}{2} + R^\star \times \vec{U_4} = \frac{\vec{V_2}}{2} + S^\star \times \vec{U_3} \tag{6.10}$$

Putting above equation in the matrix form gives:

$$\begin{bmatrix} U_{4X} & -U_{3X} \\ U_{4Y} & -U_{3Y} \end{bmatrix} \begin{bmatrix} R^\star \\ S^\star \end{bmatrix} = \begin{bmatrix} U_{4X} & -U_{3X} \\ U_{4Y} & -U_{3Y} \end{bmatrix}$$

After this matrix is solved for $R^\star$ and $S^\star$ in Matlab [71], center with respect to the local coordinate system (C.S) defined at point 3 ($P_3$) is located evaluating $R^\star$ in equation 6.8 as:

$$\vec{P_{CL}} = \frac{\vec{V_1}}{2} + R^\star\vec{U_4} \tag{6.11}$$

Lastly, coordinates of the center is transferred to the global C.S as:

$$\vec{P_C} = \vec{P_{CL}} + \vec{P_3} \tag{6.12}$$

## A.2. LOCATING CENTER OF THE CROSS SECTION AT $G$ IN ITS DEFORMED STATE

After having performed static analysis of the construct, the displacements of three initial points--$K_1, K_2, K_3$--are read from the software, and added vectorially to the initial points $(P_1, P_2, P_3)$. The deformed point coordinates are found as:

$$\dot{\vec{P_1}} = \vec{P_1} + \vec{K_1} \tag{6.13}$$

$$\dot{\vec{P_2}} = \vec{P_2} + \vec{K_3} \tag{6.14}$$

$$\dot{\vec{P_3}} = \vec{P_2} + \vec{K_3} \tag{6.15}$$

Then, a similar procedure as in 6 is followed to locate the center of deformed points, $\dot{\vec{P_C}}$. After locating the centers in undeformed and deformed states, vector defining pure translation of the center is found as:

$$W = \dot{\vec{P_C}} - \vec{P_C} \tag{6.16}$$

Axial component of the translation is found by projection of this vector onto the anatomical axis of the bone ($z$-axis), performing a dot product operation with the unit vector ($U_Z$),

$$W_Z = U_Z.W \tag{6.17}$$

and the bending angle $\theta$ is found by the equation 6.18 as:

$$\theta = COS^{-1}\left(\frac{\overrightarrow{N_P} \times \overrightarrow{\dot{N}_P}}{\|\overrightarrow{N_P}\|\|\overrightarrow{\dot{N}_P}\|}\right)\frac{180}{\pi} \qquad (6.18)$$

## A.3. CALCULATION OF STIFFNESS

The bending stiffness (B.S) in $N-m/°$ was found by evaluating the ratio of the pure bending moment $M_y = 55\ N.m$--on the mediolateral plane--to the relative angle of rotation, $\theta$, between the two ends of the interval $H$-$G$ (see Figure 3.2),

$$B.S = M_y/\theta \qquad (6.19)$$

Likewise, the axial stiffness (A.S) in $N/m$ was evaluated as the ratio of applied axial force $F_z$ to the relative axial displacement ($W_Z$) in the interval $H$-$G$ as:

$$A.S = F_Z/W_Z \qquad (6.20)$$

# APPENDIX B: PUBLICATIONS RESULTING FROM THIS THESIS

1. Okyar A.F., Bayoglu R. " The effect of loading in mechanical response predictions of bone lengthening.", Med Eng Phys, 2012, vol. 34, issue 9, pages 1362-1367, (Journal Paper).

2. Bayoglu R., Okyar A.F. " A physiologically accurate mechanical representation of the bone-implant construct under gait loads.", Sixth National Biomechanics Congress, Sakarya University Turkey, September 2012 (Conference Proceeding).

3. Okyar A.F., Bayoglu R. " Yürüme ve basamak çıkma yüklerı altında kemik-implant yapısının fizyolojik olarak doğru mekanik temsili.", 17.  Biyomedikal Mühendisliği Ulusal Toplantısı, Boğazici University, Turkey, October 2012 (Conference Proceeding)

4. Bayoglu R., Okyar A.F. " A physiologically accurate mechanical representation of a retrograde-nail bone construct under gait loading. ", Med Eng Phys, November 2012. Submitted for Publication.

## B.1. RELEVANT PUBLISHED ARTICLES

Medical Engineering & Physics 34 (2012) 1362–1367

Contents lists available at SciVerse ScienceDirect

## Medical Engineering & Physics

journal homepage: www.elsevier.com/locate/medengphy

ELSEVIER

**Technical note**

# The effect of loading in mechanical response predictions of bone lengthening

A. Fethi Okyar*, Riza Bayoglu

Department of Mechanical Engineering, Yeditepe University, Atasehir, Istanbul 34755, Turkey

ABSTRACT

Intramedullary (IM) distractor nails have become a viable alternative in bone-distraction operations. Upon stabilization of the fractured/dissected limb *via* the nail, the resulting construct accommodates the load bearing function of the otherwise healthy limb. In establishing design performance targets for these devices, *in vitro* test conditions are widely accepted leaving the *in vivo* conditions aside. However, *in vivo* device failures due to distraction forces necessitate novel modeling considerations. It is especially important to simulate the loads in limb distraction, as this brings the bone-implant construct to a totally different regime than the hip-joint contact force (Point-Force Model, PFM). In this work we used a simplified approach to incorporate ligament stretching due to limb distraction *via* self-equilibrating spring elements in a finite-element setting (spring-force model, SFM). We compared the effect of loading type on load transmission paths through the locking pins, for these two distinct loading modes, namely, SFM and PFM. The two modes illustrate entirely different load transfer regimes around the bone/nail interface region. In order to avoid high contact stresses between the nail and the bone segments, it is advisable to keep the osteotomy away from the mid-range between the pin connections. It was also seen for both loading modes that including an additional pin at a load transfer location does not significantly alter the load carried by a single pin (the additional pin rather acts as a geometric stabilizer).

© 2012 IPEM. Published by Elsevier Ltd. All rights reserved.

### 1. Introduction

Intramedullary (IM) nails are used as active distractible biomedical devices in limb-lengthening operations where the process of osteogenesis distraction accounts for new bone formation in an osteotomized bone. The correct representation of *in vivo* loading conditions of these devices are of critical importance during the design cycle. The forces that arise in the human skeleton are comprised of the body weight, ground reactions, inertial forces and internal forces. When an active biomedical device – such as an IM nail – is implanted into the body for the purpose of bone lengthening, the force system affecting the implant differs greatly between the two distinct operational phases, *viz.* the lengthening and the consolidation phases. During the lengthening phase, internal forces arise due to motions generated by the device [1]. Specifically, the increase of inter-fragment distance leads to generation of tensile forces in the callus and soft tissue, and an equivalent amount of compressive force on the bone fragments [2,3]. As the distraction reaches about 10% of the limb length, the reaction-force provided by the stretched muscles and ligaments become a primal load factor [4]. A maximum value of tensile force of nearly 1000 Newton

(N) has been reported in patients with congenitally short limbs [5]. Although, it has also been reported that large amounts of force relaxation occurs after the peak value has been reached, the model will conservatively be based on the peak load. In the literature, several clinical problems in limb-lengthening operations were reported due to excessive tension. One of these problems is mechanical failure of the implant, which is in general confined to the lower extremity zone, especially at the distal locking pin.

From a performance point-of-view, the primary function of an intramedullary nail is to provide stability and axial alignment of the osteotomy site while allowing the transmission of tensile/compressive forces from the proximal to distal fragment *via* itself [6]. The way in which loads are transferred from bone to the IM nail is critical for the design of such devices, a better understanding of which may advance the production of safer implants. In this study, we attempt to answer the following questions in regard to the above considerations: In modeling a distraction process, how should the tissue load be correctly represented? As mentioned above, during the lengthening phase loads develop internally within the tissue surrounding the femoral shaft. In a computational model, this situation could be represented by self-equilibrating preloaded linear spring elements placed between the two ends of the femur. If, however, a load equal in magnitude to the distraction force is applied instead from the hip joint (as if the loads are due to gravity), what kind of difference would that cause in the mechanical response, compared with the spring model? The

* Corresponding author. Tel.: +90 216 578 0464; fax: +90 216 578 0400.
E-mail addresses: okyar@yeditepe.edu.tr (A.F. Okyar),
riza.bayoglu@yeditepe.edu.tr (R. Bayoglu).

Figure 6.2. First page of the relavent published article 1

# REFERENCES

1. Griza, S., C. G. Zimmer, A. Reguly and T. R. Strohaecker, ``A case study of subsequential intramedullary nails failure'', *Engineering Failure Analysis*, vol. 16, pp. 728--732, 2009.

2. Knothe, U., M. L. K. Tate, K. Klaue and S. M. Perren, ``Development and testing of a new self-locking intramedullary nail system: testing of handling aspects and mechanical properties'', *Injury*, vol. 31, pp. 617--626, 2000.

3. Cheung, G., P. Zalzal, M. Bhandari, J. K. Spelt and M. Papini, ``Finite element analysis of a femoral retrograde intramedullary nail subject to gait loading'', *Med Eng Phys*, vol. 26, pp. 93--108, 2004.

4. Cai, G., M. Saleh, L. Coulton and L. Yang, ``Distraction-resisting force during tibial diaphyseal lengthening and consolidation, a study on a rabbit model'', *Clin Biomech*, vol. 19, pp. 733--737, 2004.

5. Okyar, A. and R. Bayoglu, ``The Effect of loading in mechanical response predictions of bone lengthening'', *Med Eng Phys*, vol. 34, pp. 1362--1367, 2012.

6. Chen, S. H., T. C. Yu, C. H. Chang and Y. C. Lu, ``Biomechanical analysis of retrograde intramedullary nail fixation in distal femoral fractures'', *The Knee*, vol. 15, pp. 384--389, 2008.

7. ``Static interlocking nails'', Http://dir.indiamart.com/cgi/catprdsearch .mp?ss=intramedullary+nail&pg=2 [retrieved 15 December 2012].

8. Baumgart, R., A. Betz and L. Schweiberer, ``A fully implantable motorized intramedullary nail for limb lengthening and bone transport'', *Clin Orthop Relat Res*, vol. 343, pp. 135--43, 1997.

9. Cole, J., D. Justin, T. Kasparis, D. DeVlught and C. Knobloch, ``The intramedullary skeletal kinetic distractor ISKD: first clinical results of a new intramedullary nail for lengthening of the femur and tibia'', *Injury*, vol. 32, pp. 129--139, 2001.

10. Guichet, J. M. and R. S. Casar, ``Mechanical Characterization of an Internal Gradual Elongation Nail'', *Clin Orthop Relat Res*, vol. 337, pp. 281--290, 1997.

11. Okyar, A. F., K. K. Safak and N. Egrican, ``Mechanical Design and Prototyping Considerations for an Intramedullary Nail for Extending Bone Sections'', in *Proceedings of the ASME 2010 10th Biennial Conference on Engineering Systems Design and Analysis*, pp. 1--5, ASME, July 2010.

12. Claes, L., C. Heigele, C. N. Wilke, D. Kaspar, W. Seidl, K. Margevicius and P. Augat, ``Effects of mechanical factors on the fracture healing process'', *Clin Orthop Relat Res*, vol. 355 Suppl, no. 355, pp. S132--S147, 1998.

13. Claes, L. E. and C. A. Heigele, ``Magnitudes of local stress and strain along bony surfaces predict the course and type of fracture healing'', *J Biomech*, vol. 32, pp. 255 -- 266, 1999.

14. Penzkofer, R., M. Maier, A. Nolte, G. von Oldenburg, K. Puschel, V. Buhren and P. Augat, ``Influence of intramedullary nail diameter and locking mode on the stability of tibial shaft fracture fixation'', *Arch Orthop Trauma Surg*, vol. 129, pp. 525--531, 2009.

15. WU, C. and C. SHIH, ``Interlocking nailing of distal femoral fractures - 28 patients followed for 1-2 years'', *Acta Orthop Scand*, vol. 62, pp. 342--345, 1991.

16. Boenisch, U. W., P. G. de Boer and S. F. Journeaux, ``Unreamed intramedullary tibial nailing--fatigue of locking bolts'', *Injury*, vol. 27, pp. 265--270, 1996.

17. Kneifel, T. and R. Buckley, ``A comparison of one versus two distal locking screws in tibial fractures treated with unreamed tibial nails: a prospective randomized clinical trial'', *Injury*, vol. 27, pp. 271--273, 1996.

18. Jinn, L., L. Son-Jyh, C. Po-Quang and Y. Shu-Hua, ``Stress analysis of the distal locking screws for femoral interlocking nailing'', *J Orthop Res*, vol. 19, pp. 57--63, 2001.

19. Zimmerman, K. W. and H. J. Klasen, ``Mechanical failure of intramedullary nails after fracture union'', *J Bone Joint Surg Br*, vol. 65-B, pp. 274--275, 1983.

20. Gaebler, C., S. S. Tschegg, W. Laube and V. Vecsei, ``The fatigue strength of small diameter tibial nails'', *Injury*, vol. 32, pp. 401--405, 2001.

21. Schneider, E., M. C. Michel, M. Genge, K. Zuber, R. Ganz and S. M. Perren, ``Loads acting in an intramedullary nail during fracture healing in the human femur'', *J Biomech*, vol. 34, pp. 849--857, 2001.

22. Gardner, T. N., M. Evans, H. Simpson and J. Kenwright, ``Force-displacement behaviour of biological tissue during distraction osteogenesis'', *Med Eng Phys*, vol. 20, pp. 708--715, 1998.

23. Ohnishi, I., T. Kurokawa, W. Sato and K. Nakamura, ``Measurement of the tensile forces during bone lengthening'', *Clin Biomech (Bristol, Avon)*, vol. 20, pp. 421--427, 2005.

24. Kawamura, B., S. Hosono and T. Takahashi, ``Limb lengthening by means of subcutaneous osteotomy: experimental and clinical studies'', *J Bone Joint Surg Br*, vol. 50-A, pp. 851--878, 1968.

25. Simpson, A. H. R. W., J. L. Cunningham and J. Kenwright, ``The forces which develop in the tissues during leg lengthening: a clinical study'', *J Bone Joint Surg Br*, vol. 78-B, pp. 979--983, 1996.

26. Bergmann, G., G. Deuretzbacher, M. Heller, F. Graichen, A. Rohlmann, J. Strauss and G. N. Duda, ``Hip contact forces and gait patterns from routine activities'', *J Biomech*, vol. 34, pp. 859--871, 2001.

27. Morlock, M., E. Schneider, A. Bluhm, M. Vollmer, G. Bergmann, V. Muller and M. Honl, ``Duration and frequency of every day activities in total hip patients'', *J Biomech*, vol. 34, pp. 873--881, 2001.

28. Simoes, J. A., M. A. Vaz, S. Blatcher and M. Taylor, ``Influence of head constraint and muscle forces on the strain distribution within the intact femur'', *Med Eng Phys*, vol. 22, pp. 453--459, 2000.

29. Montanini, R. and V. Filardi, ``In vitro biomechanical evaluation of antegrade femoral

nailing at early and late postoperative stages'', *Med Eng Phys*, vol. 32, pp. 889--897, 2010.

30. Schandelmaier, P., O. Farouk, C. Krettek, N. Reimers, J. Mannss and H. Tscherne, ``Biomechanics of femoral interlocking nails'', *Injury*, vol. 31, pp. 437--443, 2000.

31. Speirs, A. D., M. O. Heller, G. N. Duda and W. R. Taylor, ``Physiologically based boundary conditions in finite element modelling'', *J Biomech*, vol. 40, pp. 2318--2323, 2006.

32. Duda, G. N., M. Heller, J. Albinger, O. Schulz, E. Schneider and L. Claes, ``Influence of muscle forces on femoral strain distribution'', *J Biomech*, vol. 31, pp. 841--846, 1998.

33. ``Hip joint'', Http://www.hss.edu/hip-pain-center-hip-conditions.asp [retrieved 15 December 2012].

34. ``Knee joint'', Http://www.kneejointsreplacement.com/anatomy-of-the-knee-joint/ [retrieved 15 December 2012].

35. Britton, J. R., *Failure of cemented hip implants under complex loading: experimental and numerical analysis*, Ph.d report, Department of Mechanical Engineering, University of Ireland, March 2004.

36. Brand, R. A., D. R. Pedersen and J. A. Friederich, ``The sensitivity of muscle force predictions to changes in physiologic cross-sectional area'', *J Biomech*, vol. 19, pp. 589--596, 1986.

37. ``Muscle-locations'', Http://www.instantanatomy.net/leg/muscles/ femur.html [retrieved 15 December 2012].

38. Duda, G. N., E. Schneider and E. Y. Chao, ``Internal forces and moments in the femur during walking'', *J Biomech*, vol. 30, pp. 933--941, 1997.

39. Bergmann, G., F. Graichen, J. Siraky, H. Jendrzynski and A. Rohlmann, ``Multichannel strain gauge telemetry for orthopaedic implants'', *J Biomech*, vol. 21, pp. 169--176, 1988.

40. Graichen, F. and G. Bergmann, ``Four-channel telemetry system for in vivo measurement of hip joint forces", *Journal of Biomedical Engineering*, vol. 13, pp. 370--374, 1991.

41. ``HIP98 software", Http://www.orthoload.com/ [retrieved 15 December 2012].

42. Heller, M. O., ``Musculo-skeletal loading conditions at the hip during walking and stair climbing", *J Biomech*, vol. 34, pp. 883--893, 2001.

43. Heller, M. O., G. Bergmann, J. P. Kassi, L. Claes, N. P. Haas and G. N. Duda, ``Determination of muscle loading at the hip joint for use in pre-clinical testing", *J Biomech*, vol. 38, pp. 1155--1163, 2005.

44. Taylor, M. E., K. E. Tanner, M. A. R. Freeman and A. L. Yettram, ``Stress and strain distribution within the intact femur: compression or bending?", *Med Eng Phys*, vol. 18, pp. 122--131, 1996.

45. Polgar, K., H. S. Gill, V. M, D. W. Murray and J. J. O'Connor, ``Strain distribution within the human femur due to physiological and simplified loading: finite element analysis using the muscle standardized femur model", *Proc Inst Mech Eng H*, vol. 217, pp. 173--189, 2003.

46. Stolk, J., N. Verdonschot and R. Huiskes, ``Hip-joint and abductor-muscle forces adequately represent in vivo loading of a cemented total hip reconstruction", *J Biomech*, vol. 34, pp. 917--926, 2001.

47. Cristofolini, L., M. Juszczyk, S. Martelli, F. Taddei and M. Viceconti, ``In vitro replication of spontaneous fractures of the proximal human femur", *J Biomech*, vol. 40, pp. 2837--2845, 2007.

48. Szivek, J. A., J. B. Benjamin and P. L. Anderson, ``An experimental method for the application of lateral muscle loading and its effect on femoral strain distributions", *Med Eng Phys*, vol. 22, pp. 109 -- 116, 2000.

49. Eveleigh, R. J., ``A review of biomechanical studies of intramedullary nails", *Med Eng Phys*, vol. 17, pp. 323--331, 1995.

50. Wang, G., T. Pan, X. Peng and J. Wang, ``A new intramedullary nailing device for the treatment of femoral shaft fractures: a biomechanical study'', *Clin Biomech*, vol. 23, pp. 305--312, 2008.

51. Wang, C. J., A. L. Yettram, M. S. Yao and P. Procter, ``Finite element analysis of a Gamma nail within a fractured femur'', *Med Eng Phys*, vol. 20, pp. 677--683, 1998.

52. Kajzer, W., A. Kajzer and J. Marciniak, ``FEM analysis of expandable intramedullary nails in healthy and osteoporotic femur'', *Journal of Achievements in Materials and Manufacturing Engineering*, vol. 37, pp. 563--570, 2009.

53. Gaebler, C., A. Speitling, E. L. Milne, S. S. Tschegg, V. Vecsei and L. L. Latta, ``A new modular testing system for biomechanical evaluation of tibial intramedullary fixation devices'', *Injury*, vol. 32, pp. 708--712, 2001.

54. Kajzer, W., A. Kajzer and J. Marciniak, ``Expandable intramedullary nail - experimental biomechanical evaluation'', *Archives of Materials Science and Engineering*, vol. 41, pp. 45--52, 2010.

55. Lin, J., N. Inoue, A. Valdevit, Y. S. Hang, S. M. Hou and E. Y. Chao, ``Biomechanical Comparison of Antegrade and Retrograde Nailing of Humeral Shaft Fracture'', *Clinical Orthopaedics and Related Research*, vol. 351, pp. 203--211, 1998.

56. Ricci, W. M., C. Bellabarba, B. Evanoff, D. Herscovici, T. DiPasquale and R. Sanders, ``Retrograde Versus Antegrade Nailing of Femoral Shaft Fractures'', *Journal of Orthopaedic Trauma*, vol. 15, pp. 161--169, 2008.

57. Wang, C. J., C. J. Brown, A. L. Yettram and P. Procter, ``Intramedullary femoral nails: one or two lag screws? A preliminary study'', *Med Eng Phys*, vol. 22, pp. 613--624, 2000.

58. ``ANSYS Academic Research, Release 12.1'', .

59. ``Femur model 3rd. Generation (version 2.1)'', Http://www.biomedtown.org.

60. Viceconti, M., M. Casali, B. Massari, L. Cristofolini and S. B. A. Toni, ``The standardized femur program proposal for a reference geometry to be used for the creation of finite element models of the femur'', *J Biomech*, vol. 29, p. 1241, 1996.

61. ``ADINA R&D, Inc. Academic Research, Release 8.7.5'', .

62. Prendergast, P. J., ``Finite element models in tissue mechanics and orthopaedic implant design'', *Clin Biomech*, vol. 12, pp. 343--366, 1997.

63. Bayoglu, R. and A. F. Okyar, ``A physiologically accurate mechanical representation of the bone-implant construct under gait loads'', in *Proceedings of the sixth national biomechanics congress, Sakarya University*, p. In press, September 2012.

64. Okyar, A. F. and R. Bayoglu, ``A physiologically accurate mechanical representation of the bone-implant construct under walking and stair climbing loads'', in *Proceedings of the seventeenth national biomedical engineering meeting, Boğaziçi University*, p. In press, October 2012.

65. Reilly, D. T., A. H. Burstein and V. H. Frankel, ``The elastic modulus for bone'', *J Biomech*, vol. 7, pp. 271--275, 1974.

66. Panagiotopoulou, O., S. D. Wilshin, E. J. Rayfield, S. J. Shefelbine and J. RHutchinson, ``What makes an accurate and reliable subject-specific finite element model? A case study of an elephant femur'', *J R Soc Interface*, vol. 9, pp. 351--361, 2012.

67. Ramos, A. and J. A. Simoes, ``Tetrahedral versus hexahedral finite elements in numerical modelling of the proximal femur'', *Med Eng Phys*, vol. 28, pp. 916--924, 2006.

68. Huiskes, R. and E. Y. S. Chao, ``A survey of finite element analysis in orthopedic biomechanics: The first decade'', *J Biomech*, vol. 16, pp. 385--409, 1983.

69. Phillips, A. T. M., ``The femur as a musculo-skeletal construct: A free boundary condition modelling approach'', *Med Eng Phys*, vol. 31, pp. 673--680, 2009.

70. Paul, J. P., ``Stress and strain distribution within the intact femur: compression or

bending? by Taylor et al.", *Med Eng Phys*, vol. 19, p. 97, 1997.

71.  ``Matlab (2009a, The Mathworks, Natick, Massachusetts, U.S.A.)'', .